Physical Layer Security Aided Wireless Interference Networks in the Presence of Strong Eavesdropper Channels

Zhichao Sheng, Hoang Duong Tuan, Ali Arshad Nasir, H. Vincent Poor, and Eryk Dutkiewicz

***Abstract*—Under both long (infinite) and short (finite) blocklength transmissions, this paper considers physical layer security for a wireless interference network of multiple transmitter-user pairs, which is overheard by multiple eavesdroppers (EVs). The EVs are assumed to have better channel conditions than the legitimate users (UEs), making the conventional transmission unsecured. The paper develops a novel time-fraction based transmission, under which the information is transmitted to the UEs within a fraction of the time slot and artificial noise (AN) is transmitted within the remaining fraction to counter the strong EVs' channels. Based on channel distribution information of UEs and EVs, the joint design of transmit beamforming, time fractions and AN power allocation to maximize the worst users' secrecy rate is formulated in terms of nonconvex problems. Path-following algorithms of low complexity and rapid convergence are proposed for their solution. Simulations are provided to demonstrate the viability of the proposed methodology.**

***Index Terms*—Interference network, physical layer security, outage-aware beamforming, nonconvex optimization, path-following algorithms.**

I. INTRODUCTION

Information security is very critical in wireless communication as the transmitted messages are vulnerable to be eavesdropped by unintended receivers in close proximity [1]. Physical layer security (PLS) [2]–[5] is a promising solution to address information security. Secrecy rate, often given as the difference between the legitimate user's rate and the eavesdropper's rate, is an important metric in PLS. Based on the perfect or imperfect channel state information (CSI) of the legitimate users (UEs) and eavesdroppers (EVs) at the transmitter, secrecy rate optimization has been considered in [6]–[13]. It is more practical to only assume channel distribution information (CDI) of EVs at the transmitter as done in [14]–[18], which however could consider only a simple scenario with a single EV. Apparently, it is very challenging to reach reasonable secrecy rates when the EVs have better channel conditions than the UEs.

Recently, ultra-reliable and low-latency communication (URLLC) [19] has attracted significant attention thanks to its potential applications in the internet-of-things (IoT), where low-latency and high reliability are achieved by short (finite) blocklength (FBL) transmission with tight error-probability constraints. In the FBL regime, the secrecy rate is a quite complicated function of the signal-to-noise ratio (SNR) [20], [21]. Based on the perfect CSI of UEs and EVs, the joint power and bandwidth allocation to maximize the weighted sum secrecy rate with a single EV was addressed in [22] by using d.c. (difference of two convex function) iterations [23], while the beamforming design to minimize the total transmit power under quality-of-service (QoS) in terms of users' URLLC secrecy rates was addressed in [24] by using semi-definite relaxation, which in the end may not lead to a feasible point and thus is not computationally flexible [25]. All these works assume that UEs have much better channel conditions than EVs.

Against the above background, this paper aims to develop PLS for a network of multiple transmitter-user (TR-UE) pairs overheard by multiple EVs, who have better channel conditions than the UEs. CDI of the UEs and EVs is assumed to be known at the transmitters. The contribution of this paper is two-fold:

- To counter strong EVs' channels, we adopt a time-fraction based transmission [5], [26], under which the information is transmitted to the UEs during a fraction of the time slot, while artificial noise (AN) is transmitted within the remaining fraction. The time fractions as a secrete key is shared among the UEs but not the EVs and thus the AN is expected to degrade the EVs' rate to improve the UEs' secrecy rates. In this sense, the technique we propose here is a hybrid between physical layer and shared-secret security methods. Accordingly, the problem of joint optimization in the time fraction allocation, transmit beamforming, and AN power allocation to maximize the minimum secrecy outage probability is formulated and then computed by a novel path-following algorithm of rapid convergence, which invokes a convex problem of low computational complexity at each iteration to generate a better feasible point.
- The same scenario with strong EVs' channels is also

The work is supported in part by National Natural Science Foundation of China (NSFC) under Grant 61901254, in part by the Australian Research Council's Discovery Projects under Project DP190102501, and in part by U.S. National Science Foundation under Grant CCF-1908308.

Zhichao Sheng is with the Key Laboratory of Specialty Fiber Optics and Optical Access Networks, Shanghai Institute for Advanced Communication and Data Science, Shanghai University, Shanghai 200444, China (email: zcsheng@shu.edu.cn).

Hoang Duong Tuan and Eryk Dutkiewicz are with the School of Electrical and Data Engineering, University of Technology Sydney, Broadway, NSW 2007, Australia (email: Tuan.Hoang@uts.edu.au, Eryk.Dutkiewicz@uts.edu.au);

Ali Arshad Nasir is with the Department of Electrical Engineering, King Fahd University of Petroleum and Minerals (KFUPM), Dhahran 31261, Saudi Arabia (email: anasir@kfupm.edu.sa);

H. Vincent Poor is with the Department of Electrical Engineering, Princeton University, Princeton, NJ 08544, USA (email: poor@princeton.edu).

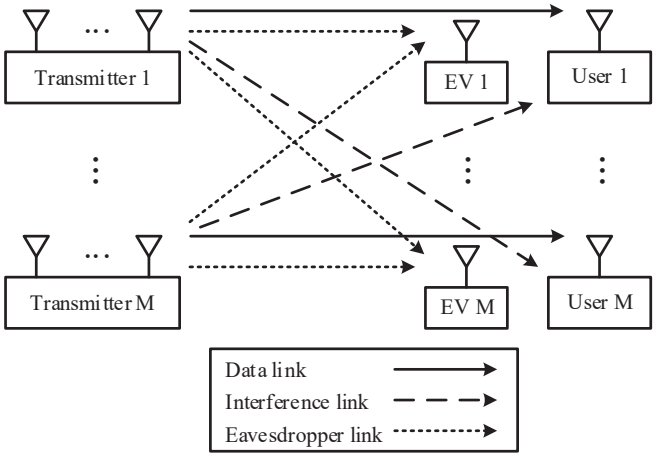

Fig. 1. System model.

considered in the FBL regime. As expected, the problem of maximizing the minimum secrecy outage probability is much more computationally challenging than that in the long blocklength (LBL) regime due to the presence of channel dispersion for both UEs and EVs in the definition of the secrecy outage probability. Another path-following algorithm, which iterates a simple convex problem of low computational complexity to generate feasible points and converges rapidly at least to a locally optimal solution, is developed.

The paper is organized as follows. Section II is devoted to PLS solution against strong EVs' channels in the LBL regime, while Section III is devoted to PLS solution against strong EVs' channels in the FBL regime. Simulation results are presented in Section IV while the conclusions are given in Section V.

Notation. Optimization decision variables are boldfaced. The notation $\sum_{j\neq i}^{M}$ refers to the summation taking over the index set $\mathcal{M}\backslash\{i\}$ for $\mathcal{M} \triangleq \{1,\ldots,M\}$. $\mathcal{CN}(0, I_{N_t})$ is the set of complex Gaussian vector in $\mathbb{C}^{N_t}$ of zero mean and identity covariance matrix I_{N_t} of size $N_t \times N_t$, while $\mathcal{N}(0,1)$ is the set of real scalar Gaussian variables of zero mean and unit covariance. $(.)^H$ and $\|\cdot\|$ stand for the Hermitian transpose and Euclidean norm of a vector, while $|\cdot|$ and $\Re\{.\}$ stand for the magnitude and the real part of a complex number. $\mathbb{C}$ and $\mathbb{R}$ denote the sets of complex and real numbers, respectively.

II. Secure LBL regime

Consider a multiple-input single output (MISO) wireless network of M TR-UE pairs, which is overheard by M EVs, as depicted in Fig. 1. Each transmitter (TR) is equipped with N_t transmit antennas while the UEs and EVs are equipped with a single antenna. Unlike the existing works, we assume that EVs are in better channel conditions than the UEs because EVs are located nearer to the TRs. In addition, we only assume that CDI of the UEs and EVs is available at the transmitters. To counter the EVs' strong channels, we apply a time-fraction based transmission [5], [26], which allocates a fraction $0 < 1/\boldsymbol{t}_1 < 1$ of the time slot for information transmission and the remaining fraction $0 < 1/\boldsymbol{t}_2 < 1$ for AN transmission to confuse the EVs. The information symbol s_i for UE i, which is normalized to $\mathbb{E}\{|s_i|^2\} = 1$, is beamformed by the vector $\mathbf{w}_i \in \mathbb{C}^{N_t}$. The signal received at UE i during the time-fraction $1/\boldsymbol{t}_1$ is

$$y_i = \tilde{h}_{ii}^H \mathbf{w}_i s_i + \sum_{j\neq i}^{M} \tilde{h}_{ji}^H \mathbf{w}_j s_j + n_i, i \in \mathcal{M}, \tag{1}$$

where $\tilde{h}_{ji} \in \mathbb{C}^{N_t}$ is the vector channel from TR j to UE i and $n_i \in \mathbb{C}$ is white Gaussian background noise with power $\sigma_i^2 \triangleq \sigma^2\mathcal{B}$ upon the noise power spectral density (noise power per unit bandwidth) σ^2 and the communication bandwidth $\mathcal{B}$.

The channel $\tilde{h}_{ji}$ from TR j to UE i is modeled as

$$\tilde{h}_{ji} = h_{ji} + \delta\chi_{ji}, \tag{2}$$

where $h_{ji} = \sqrt{\beta_{ji}}\phi_{ji}$ with the deterministic quantities $\sqrt{\beta_{ji}}$ and $\phi_{ji} \in \mathbb{C}^{N_t}$ respectively representing the large-scale fading from TR j to EV i and a normalized small-scale fading channel, and $\delta\chi_{ji}$ with the deterministic $0 < \delta \ll 1$ and the random $\chi_{ji} \in \mathcal{CN}(0, I_{N_t})$ representing the channel error in channel state estimation.

The signal received at EV k during the time-fraction $1/\boldsymbol{t}_1$ is

$$y_{1k}^E = \sum_{i=1}^{M} h_{ik,e}^H \mathbf{w}_i s_i + n_e, \tag{3}$$

where $h_{ik,e} \in \mathbb{C}^{N_t}$ is the vector channel from TR i to EV k and $n_e \in \mathbb{C}$ is white Gaussian background noise with power $\sigma_e^2 \triangleq \sigma^2\mathcal{B}$. The signal received at EV k during the time-fraction $1/\boldsymbol{t}_2$ is

$$y_{2k}^E = \sum_{i=1}^{M} h_{ik,e}^H \Delta_i + n_e, \tag{4}$$

where $\Delta_i \in \mathcal{CN}(0, \boldsymbol{x}_i^2 I)$ is AN of power $\boldsymbol{x}_i^2$ that TR i sends to confuse EVs. The channel $h_{jk,e}$ from TR j to EV k is modeled by

$$h_{jk,e} = \sqrt{\beta_{jk,e}}\chi_{jk}^E, \tag{5}$$

where the deterministic $\sqrt{\beta_{jk,e}}$ represents the large-scale fading from TR j to EV k, and the random $\chi_{jk}^E \in \mathcal{CN}(0, I)$ represents the small-scale fading in the channel.

For $\mathbf{w} \triangleq \{\mathbf{w}_i \ : \ i \in \mathcal{M}\}$, introduce the scalar variables $\mathbf{R}_i > 0$ to implicitly define the UE i's rate in nats/sec through the outage probability as

$$\varphi_{i,o}(\mathbf{w}, \boldsymbol{t}_1) \triangleq \frac{1}{\boldsymbol{t}_1} \times \max_{\mathbf{R}_i} \{\ln(1+\mathbf{R}_i) \ : \tag{6a}$$

$$\text{Prob}\left(\frac{|h_{ii}^H \mathbf{w}_i|^2}{\delta^2|\chi_{ii}^H \mathbf{w}_i|^2 + \sum_{j\neq i}^{M}|(h_{ji}+\delta\chi_{ji})^H\mathbf{w}_j|^2 + \sigma_i^2} < \mathbf{R}_i\right) < \epsilon\} \tag{6b}$$

for $\epsilon > 0$, where we assume that information about the time-fraction is sent via secure control channels to all the UEs.

According to [17, Prop. 1], we have

$$\varphi_{i,o}(\mathbf{w}, \boldsymbol{t}_1) \geq \frac{1}{\boldsymbol{t}_1} \times \max \left\{ \ln(1+\mathbf{R}_i) \ :$$

$$\delta\left[\delta_M n_{\min}(\mathbf{w}) + \frac{M-1}{2} n_{\min}(\mathbf{w}) \times \ln\frac{\psi_i(\mathbf{w},\mathbf{R}_i)}{n_{\min}(\mathbf{w})}\right] \le \psi_i(\mathbf{w},\mathbf{R}_i)\Big\}, \quad (7)$$

where

$$\psi_i(\mathbf{w},\mathbf{R}_i) \triangleq \frac{|h_{ii}^H\mathbf{w}_i|^2}{\mathbf{R}_i} - \left[(1-\delta)^{-1}\sum_{j\neq i}^{M}|h_{ji}^H\mathbf{w}_j|^2 + \sigma_i^2\right], \quad (8)$$

$$0 < \delta_M \triangleq -\left(\ln\epsilon - \ln M + \frac{1}{M}\sum_{i=1}^{M}\ln\Gamma(i) + \frac{M-1}{2}\ln\delta\right) = \ln\epsilon^{-1} + \ln M - \frac{1}{M}\sum_{i=1}^{M}\ln\Gamma(i) + \frac{M-1}{2}\ln\delta^{-1}, \quad (9)$$

and

$$n_{\min}(\mathbf{w}) \triangleq \min_{i\in\mathcal{M}} ||\mathbf{w}_i||^2. \quad (10)$$

Since the EVs overhear the time-slot-wise signal and they are not aware of the time-fraction of information and AN transmission, the signal y_{2k}^E in (4) is treated as an additional noise to jam the EVs. The noise power in decoding s_i by EV k is

$$\frac{1}{\boldsymbol{t}_2}\sum_{i=1}^{M}\beta_{ik,e}\boldsymbol{x}_i^2 + \sigma_e^2. \quad (11)$$

For $\boldsymbol{x} \triangleq \{\boldsymbol{x}_i \ : \ i\in\mathcal{M}\}$, introduce the scalar variable $\mathbf{r}_{ik} > 0$ and the function

$$g_{ik}(\mathbf{r}_{ik},\mathbf{w},\boldsymbol{x},\boldsymbol{t}_2) \triangleq \beta_{ik,e}\ln(1-\epsilon_{EV}) + \left(\frac{1}{\boldsymbol{t}_2}\sum_{i=1}^{M}\beta_{ik,e}\boldsymbol{x}_i^2 + \sigma_e^2\right)\frac{\mathbf{r}_{ik}}{\|\mathbf{w}_i\|^2} + \beta_{ik,e}\sum_{j\neq i}^{M}\ln\left(1 + \frac{\mathbf{r}_{ik}\beta_{jk,e}\|\mathbf{w}_j\|^2}{\beta_{ik,e}\|\mathbf{w}_i\|^2}\right) \quad (12)$$

for $\epsilon_{EV} > 0$. Regarding s_i, the information leakage to EV k is defined through the outage probability as[1]

$$\max\{\ln(1+\mathbf{r}_{ik}) \ : \quad (13a)$$

$$\text{Prob}\left(\frac{\beta_{ik,e}|(\chi_{ik}^E)^H\mathbf{w}_i|^2}{\sum_{j\neq i}^{M}\beta_{jk,e}|(\chi_{jk}^E)^H\mathbf{w}_j|^2 + \frac{1}{\boldsymbol{t}_2}\sum_{i=1}^{M}\beta_{ik,e}\boldsymbol{x}_i^2 + \sigma_e^2} < \mathbf{r}_{ik}\right) < \epsilon_{EV}\}, \quad (13b)$$

which is [16]

$$\max_{\mathbf{r}_{ik}\ge 0} \ \ln(1+\mathbf{r}_{ik}) \quad \text{s.t.} \quad g_{ik}(\mathbf{r}_{ik},\mathbf{w},\boldsymbol{x},\boldsymbol{t}_2) \ge 0. \quad (14)$$

UE i's secrecy rate is now given by

$$\varphi_i(\mathbf{R}_i,\mathbf{r}_i,\boldsymbol{t}_1) \triangleq \rho_i(\mathbf{R}_i,\boldsymbol{t}_1) - \max_{k\in\mathcal{M}}\rho_{E,ik}(\mathbf{r}_{ik}), \quad (15)$$

where

$$\rho_i(\mathbf{R}_i,\boldsymbol{t}_1) \triangleq \frac{1}{\boldsymbol{t}_1}\ln(1+\mathbf{R}_i) \quad (16)$$

[1]The reader is referred to [27] for a metric linking the concept of secrecy outage with the decodability of messages at EVs.

is UE i's rate, and

$$\rho_{E,ik}(\mathbf{r}_{ik}) \triangleq \ln(1+\mathbf{r}_{ik}) \quad (17)$$

is EV k's rate in decoding the symbol s_i. Therefore,

$$\rho_{E,i}(\mathbf{r}_i) \triangleq \max_{k\in\mathcal{M}}\ln(1+\mathbf{r}_{ik})$$

for $\mathbf{r}_i \triangleq \{\mathbf{r}_{ik} \ : \ k\in\mathcal{M}\}$, is the EVs' maximal rate in decoding the symbol s_i.

Thus, for $\mathbf{R} \triangleq \{\mathbf{R}_i \ : \ i\in\mathcal{M}\}$, $\mathbf{r} \triangleq \{\mathbf{r}_i \ : \ i\in\mathcal{M}\}$, and $\boldsymbol{t} \triangleq (\boldsymbol{t}_1,\boldsymbol{t}_2)$, the max-min secrecy rate optimization problem can be formulated as follows:

$$\max_{\boldsymbol{w},\boldsymbol{x},\boldsymbol{t},\mathbf{R},\mathbf{r}} \ \Phi(\mathbf{R},\mathbf{r},\boldsymbol{t}_1) \triangleq \min_{i\in\mathcal{M}} \ \varphi_i(\mathbf{R}_i,\mathbf{r}_i,\boldsymbol{t}_1) \quad \text{s.t.} \quad (18a)$$

$$\frac{\|\mathbf{w}_i\|^2}{\boldsymbol{t}_1} + \frac{\boldsymbol{x}_i^2}{\boldsymbol{t}_2} \le P_i, i\in\mathcal{M}, \quad (18b)$$

$$\|\mathbf{w}_i\|^2 \le 3P_i, \boldsymbol{x}_i^2 \le 3P_i, i\in\mathcal{M}, \quad (18c)$$

$$\frac{1}{\boldsymbol{t}_1} + \frac{1}{\boldsymbol{t}_2} \le 1, \boldsymbol{t}_1 \ge 1, \boldsymbol{t}_2 \ge 1, \quad (18d)$$

$$\mathbf{R}_i > 0, \mathbf{r}_i > 0, i\in\mathcal{M}, \quad (18e)$$

$$\psi_i(\mathbf{w},\mathbf{R}_i) > 0, i\in\mathcal{M}, \quad (18f)$$

$$\delta\left[\delta_M n_{\min}(\mathbf{w}) + \frac{M-1}{2} n_{\min}(\mathbf{w})\ln\frac{\psi_i(\mathbf{w},\mathbf{R}_i)}{n_{\min}(\mathbf{w})}\right] \le \psi_i(\mathbf{w},\mathbf{R}_i), i\in\mathcal{M}, \quad (18g)$$

$$g_{ik}(\mathbf{r}_{ik},\mathbf{w},\boldsymbol{x},\boldsymbol{t}_2) \ge 0, \ i\in\mathcal{M}, k\in\mathcal{M}, \quad (18h)$$

where P_i defines the limit of transmission power at TR i. In what follows, we explain how to handle the non-concave objective function in (18) and three nonconvex constraints (18f), (18g) and (18h), which make (18) a nonconvex problem and thus computationally challenging.

In order to solve (18), we adopt a path-following algorithm, which is an iterative algorithm and generates a sequence of improved feasible points for (18) at each iteration and at least converges to a locally optimal solution of (18). Let $(w^{(\kappa)},x^{(\kappa)},t^{(\kappa)},R^{(\kappa)},r^{(\kappa)})$ be a feasible point for (18) found from the $(\kappa-1)$th iteration.[2] We first handle the non-concave objective function in (18). By applying the inequality (81) in the appendix for $z=\mathbf{R}_i$, $\tau=\boldsymbol{t}_1$ and $\bar{z}=R_i^{(\kappa)}$, $\bar{\tau}=t_1^{(\kappa)}$, the UE i' rate function $\rho_i(\mathbf{R}_i,\boldsymbol{t}_1)$ is lower bounded by a concave function as

$$\rho_i(\mathbf{R}_i,\boldsymbol{t}_1) \ge \rho_i^{(\kappa)}(\mathbf{R}_i,\boldsymbol{t}_1) \triangleq \frac{2}{t_1^{(\kappa)}}\ln(1+R_i^{(\kappa)}) + \frac{R_i^{(\kappa)}}{t_1^{(\kappa)}(R_i^{(\kappa)}+1)} - \frac{(R_i^{(\kappa)})^2}{t_1^{(\kappa)}(R_i^{(\kappa)}+1)}\frac{1}{\mathbf{R}_i} - \frac{\boldsymbol{t}_1}{(t_1^{(\kappa)})^2}\ln(1+R_i^{(\kappa)}), \quad (19)$$

while by applying the inequality (79) in the appendix for $z=\mathbf{r}_{ik}$ and $\bar{z}=r_{ik}^{(\kappa)}$, the EV k' rate function $\rho_{E,ik}(\mathbf{r}_{ik})$ is upper bounded by a convex function as

$$\rho_{E,ik}(\mathbf{r}_{ik}) \le \rho_{E,ik}^{(\kappa)}(\mathbf{r}_{ik})$$

[2]It is also called majoration-minimization in some popular literatures.

$$\triangleq \ln(1+r_{ik}^{(\kappa)}) - \frac{r_{ik}^{(\kappa)}}{r_{ik}^{(\kappa)}+1} + \frac{\mathbf{r}_{ik}}{r_{ik}^{(\kappa)}+1}. \quad (20)$$

Hence, the secrecy rate function $\varphi_i(\mathbf{R}_i, \mathbf{r}_i, \boldsymbol{t}_1)$ is lower bounded by a concave function as[3]

$$\begin{aligned}\varphi_i(\mathbf{R}_i, \mathbf{r}_i, \boldsymbol{t}_1) &\geq \varphi_i^{(\kappa)}(\mathbf{R}_i, \mathbf{r}_i, \boldsymbol{t}_1) \\ &\triangleq \rho_i^{(\kappa)}(\mathbf{R}_i, \boldsymbol{t}_1) - \max_{k\in\mathcal{M}} \rho_{E,ik}^{(\kappa)}(\mathbf{r}_{ik}).\end{aligned}$$

The objective $\Phi(\mathbf{R}, \mathbf{r}, \boldsymbol{t}_1)$ in (18) is thus bounded by a concave function as[4]

$$\Phi(\mathbf{R}, \mathbf{r}, \boldsymbol{t}_1) \geq \Phi^{(\kappa)}(\mathbf{R}, \mathbf{r}, \boldsymbol{t}_1) \triangleq \min_{i\in\mathcal{M}} \varphi_i^{(\kappa)}(\mathbf{R}_i, \mathbf{r}_i, \boldsymbol{t}_1). \quad (21)$$

Next, we have to address the nonconvex constraints (18f), (18g), and (18h). Note that $|h_{ii}^H \mathbf{w}_i|^2/\mathbf{R}_i$ is a convex function, so

$$\frac{|h_{ii}^H \mathbf{w}_i|^2}{\mathbf{R}_i} \geq \ell_i^{(\kappa)}(\mathbf{w}_i, \mathbf{R}_i) \quad (22)$$

$$\triangleq \frac{2\Re\Big\{(w_i^{(\kappa)})^H h_{ii} h_{ii}^H \mathbf{w}_i\Big\}}{R_i^{(\kappa)}} - \frac{\mathbf{R}_i |h_{ii}^H w_i^{(\kappa)}|^2}{(R_i^{(\kappa)})^2}, \quad (23)$$

because $\ell_i^{(\kappa)}(\mathbf{w}_i, \mathbf{R}_i)$ is the linearization of $|h_{ii}^H \mathbf{w}_i|^2/\mathbf{R}_i$ at $(w_i^{(\kappa)}, R_i^{(\kappa)})$ [28]. Therefore, the nonconvex constraint (18f) is innerly approximated by the following convex constraint

$$\ell_i^{(\kappa)}(\mathbf{w}_i, \mathbf{R}_i) > (1-\delta)^{-1} \sum_{j\neq i}^{M} |h_{ji}^H \mathbf{w}_j|^2 + \sigma_i^2. \quad (24)$$

Furthermore, applying the inequality (78) in the appendix for $z = \psi_i(\mathbf{w}, \mathbf{R}_i)/n_{\min}(\mathbf{w})$ and $\chi_i^{(\kappa)} \triangleq \psi_i(w^{(\kappa)}, R_i^{(\kappa)})/n_{\min}(w^{(\kappa)})$ yields

$$\ln \frac{\psi_i(\mathbf{w}, \mathbf{R}_i)}{n_{\min}(\mathbf{w})} \leq \ln(\chi_i^{(\kappa)}) - 1 + \frac{\psi_i(\mathbf{w}, \mathbf{R}_i)}{\chi_i^{(\kappa)} n_{\min}(\mathbf{w})},$$

or equivalently,

$$\begin{aligned} n_{\min}(\mathbf{w}) \ln \frac{\psi_i(\mathbf{w}, \mathbf{R}_i)}{n_{\min}(\mathbf{w})} &\leq \Big(\ln(\chi_i^{(\kappa)}) - 1\Big) n_{\min}(\mathbf{w}) \\ &\quad + \frac{\psi_i(\mathbf{w}, \mathbf{R}_i)}{\chi_i^{(\kappa)}}.\end{aligned}$$

For $\Delta \triangleq \delta(M-1)/2$, the nonconvex constraint (18g) is thus innerly approximated by the following constraint

$$\left(\ln(\chi_i^{(\kappa)}) - 1 + \frac{\delta_M \delta}{\Delta}\right) n_{\min}(\mathbf{w}) \leq \left(\frac{1}{\Delta} - \frac{1}{\chi_i^{(\kappa)}}\right) \psi_i(\mathbf{w}, \mathbf{R}_i), \quad (25)$$

which is still nonconvex.

For

$$i^{(\kappa)} \triangleq \arg\min_{i\in\mathcal{M}} ||w_i^{(\kappa)}||^2,$$

i.e.

$$||w_{i^{(\kappa)}}^{(\kappa)}||^2 = n_{\min}(w^{(\kappa)}),$$

it follows from the definition (10) of the function $n_{\min}(\mathbf{w})$ that

$$n_{\min}(\mathbf{w}) \leq ||\mathbf{w}_{i^{(\kappa)}}||^2 \ \forall \ \mathbf{w}. \quad (26)$$

Also, from the definition (8) and the inequality (22), it follows that

$$\psi_i(\mathbf{w}, \mathbf{R}_i) \geq \psi_i^{(\kappa)}(\mathbf{w}, \mathbf{R}_i) \quad (27)$$

$$\triangleq \ell_i^{(\kappa)}(\mathbf{w}_i, \mathbf{R}_i) - (1-\delta)^{-1} \sum_{j\neq i}^{M} |\bar{h}_{ji}^H \mathbf{w}_j|^2 - \sigma_i^2. \quad (28)$$

Observing that $\ln(\chi_i^{(\kappa)}) - 1 + \frac{\delta_M \delta}{\Delta} \geq 0$ and $\frac{1}{\Delta} - \frac{1}{\chi_i^{(\kappa)}} \geq 0$, we use (26) and (27) to derive the following inner convex approximation of the nonconvex constraint (25) for each $i \in \mathcal{M}$:

$$\begin{aligned}\left(\ln(\chi_i^{(\kappa)}) - 1 + \frac{\delta_M \delta}{\Delta}\right) ||\mathbf{w}_{i^{(\kappa)}}||^2 \quad &\leq \\ \left(\frac{1}{\Delta} - \frac{1}{\chi_i^{(\kappa)}}\right) \psi_i^{(\kappa)}(\mathbf{w}, \mathbf{R}_i), \quad (29)\end{aligned}$$

which is also an inner convex approximation of the nonconvex constraint (18g).

To handle the nonconvex constraint (18h) for the function g_{ik} defined from (12), let us recall the following inequality [18, (8)]:

$$\ln\left(1 + \frac{\mathbf{r}_{ik}\beta_{jk,e}\|\mathbf{w}_j\|^2}{\beta_{ik,e}\|\mathbf{w}_i\|^2}\right) \geq \lambda_{ijk}^{(\kappa)}(\mathbf{r}_{ik}, \mathbf{w}_j, \mathbf{w}_i) \quad (30)$$

over the trust region

$$2\Re\{(w_j^{(\kappa)})^H \mathbf{w}_j\} - \|w_j^{(\kappa)}\|^2 > 0 \quad (31)$$

for

$$\begin{aligned}\lambda_{ijk}^{(\kappa)}(\mathbf{r}_{ik}, \mathbf{w}_j, \mathbf{w}_i) \quad &\triangleq \\ \ln(1+\chi_{ijk}^{(\kappa)}) + 2\xi_{ijk}^{(\kappa)} \\ -\xi_{ijk}^{(\kappa)}\left(\frac{r_{ik}^{(\kappa)}\|w_j^{(\kappa)}\|^2}{\mathbf{r}_{ik}(2\Re\{(w_j^{(\kappa)})^H \mathbf{w}_j\} - \|w_j^{(\kappa)}\|^2)} + \frac{\|\mathbf{w}_i\|^2}{\|w_i^{(\kappa)}\|^2}\right), \quad (32)\end{aligned}$$

with $\chi_{ijk}^{(\kappa)} \triangleq r_{ik}^{(\kappa)}\beta_{jk,e}\|w_j^{(\kappa)}\|^2/\beta_{ik,e}\|w_i^{(\kappa)}\|^2$ and $\xi_{ijk}^{(\kappa)} \triangleq \chi_{ijk}^{(\kappa)}/(\chi_{ijk}^{(\kappa)}+1)$.

By introducing the scalar variables $\boldsymbol{\eta}_{ik}$, $i \in \mathcal{M}$, $k \in \mathcal{M}$, satisfying the constraint

$$\left(\frac{1}{\boldsymbol{t}_2}\sum_{i=1}^{M} \beta_{ik,e}\boldsymbol{x}_i^2 + \sigma_e^2\right) \frac{\mathbf{r}_{ik}}{\|\mathbf{w}_i\|^2} \geq \boldsymbol{\eta}_{ik}, i \in \mathcal{M}, k \in \mathcal{M}, \quad (33)$$

it follows from (12) and (30) and (33) that

$$\begin{aligned} g_{ik}(\mathbf{r}_{ik}, \mathbf{w}, \boldsymbol{x}, \boldsymbol{t}_2) \quad &\geq \\ \beta_{ik,e}\ln(1-\epsilon_{EV}) + \boldsymbol{\eta}_{ik} + \beta_{ik,e}\sum_{j\neq i}^{M} \lambda_{ijk}^{(\kappa)}(\mathbf{r}_{ik}, \mathbf{w}_j, \mathbf{w}_i).\end{aligned}$$

As such, the nonconvex constraint (18h) is innerly approximated by the convex constraint

$$\beta_{ik,e}\ln(1-\epsilon_{EV}) + \boldsymbol{\eta}_{ik}$$

[3] $\max_{k\in\mathcal{M}} \rho_{E,ik}^{(\kappa)}(\mathbf{r}_{ik})$ is convex as pointwise maximum of convex functions $\rho_{E,ik}^{(\kappa)}(\mathbf{r}_{ik})$ [28]

[4] $\Phi^{(\kappa)}(\mathbf{R}, \mathbf{r}, \boldsymbol{t}_1)$ is concave as pointwise minimum of concave functions $\varphi_i^{(\kappa)}(\mathbf{R}_i, \mathbf{r}_i, \boldsymbol{t}_1)$ [28]

$$+\beta_{ik,e}\sum_{j\neq i}^{M}\lambda_{ijk}^{(\kappa)}(\mathbf{r}_{ik},\mathbf{w}_j,\mathbf{w}_i) \quad \geq \quad 0,\ i\in\mathcal{M},k\in\mathcal{M}. \tag{34}$$

As (33) is a nonconvex constraint, we need to provide its inner convex approximation. Note that

$$(33)\Leftrightarrow \frac{\mathbf{r}_{ik}}{\|\mathbf{w}_i\|^2}\geq\frac{\boldsymbol{t}_2\boldsymbol{\eta}_{ik}}{\sum_{i=1}^{M}\beta_{ik,e}\boldsymbol{x}_i^2+\sigma_e^2\boldsymbol{t}_2}, i\in\mathcal{M},k\in\mathcal{M}. \tag{35}$$

By applying the inequality (82) in the appendix for $z=\mathbf{r}_{ik}$, $\tau=||\mathbf{w}_i||$, and $\bar{z}=r_{ik}^{(\kappa)}$, $\bar{\tau}=||w_i^{(\kappa)}||$, we obtain

$$\frac{\mathbf{r}_{ik}}{\|\mathbf{w}_i\|^2}\geq\beta_{ik}^{(\kappa)}(\mathbf{r}_{ik},\mathbf{w}_i),$$

where

$$\begin{aligned}\beta_{ik}^{(\kappa)}(\mathbf{r}_{ik},\mathbf{w}_i) \quad \triangleq \quad & 2\left(\sqrt{r_{ik}^{(\kappa)}}/\|w_i^{(\kappa)}\|^2\right)\sqrt{\mathbf{r}_{ik}}\\ & -\left(r_{ik}^{(\kappa)}/\|w_i^{(\kappa)}\|^4\right)\|\mathbf{w}_i\|^2,\end{aligned}$$

which is a concave function. Furthermore,

$$\boldsymbol{t}_2\boldsymbol{\eta}_{ik}\leq\frac{\eta_{ik}^{(\kappa)}t_2^{(\kappa)}}{4}\left(\frac{\boldsymbol{t}_2}{t_2^{(\kappa)}}+\frac{\boldsymbol{\eta}_{ik}}{\eta_{ik}^{(\kappa)}}\right)^2$$

for

$$\eta_{ik}^{(\kappa)}\triangleq\left(\frac{1}{t_2^{(\kappa)}}\sum_{i=1}^{M}\beta_{ik,e}(x_i^{(\kappa)})^2+\sigma_e^2\right)\frac{r_{ik}^{(\kappa)}}{\|w_i^{(\kappa)}\|^2},$$

and

$$\sum_{i=1}^{M}\beta_{ik,e}(\boldsymbol{x}_i)^2\geq\sum_{i=1}^{M}\beta_{ik,e}(2x_i^{(\kappa)}\boldsymbol{x}_i-(x_i^{(\kappa)})^2).$$

The nonconvex constraint (35)/(33) is thus innerly approximated by the following convex constraint

$$\begin{aligned}&\beta_{ik}^{(\kappa)}(\mathbf{r}_{ik},\mathbf{w}_i) \quad \geq\\ &\frac{\eta_{ik}^{(\kappa)}t_2^{(\kappa)}\left(\frac{\boldsymbol{t}_2}{t_2^{(\kappa)}}+\frac{\boldsymbol{\eta}_{ik}}{\eta_{ik}^{(\kappa)}}\right)^2}{4\left(\sum_{i=1}^{M}\beta_{ik,e}(2x_i^{(\kappa)}\boldsymbol{x}_i-(x_i^{(\kappa)})^2)+\sigma_e^2\boldsymbol{t}_2\right)},\\ &\qquad i\in\mathcal{M},k\in\mathcal{M},\end{aligned} \tag{36}$$

under the trust region

$$\sum_{i=1}^{M}\beta_{ik,e}(2x_i^{(\kappa)}\boldsymbol{x}_i-(x_i^{(\kappa)})^2)+\sigma_e^2\boldsymbol{t}_2>0,k\in\mathcal{M}. \tag{37}$$

Initialized from a feasible point $(w^{(0)},x^{(0)},t^{(0)},R^{(0)},r^{(0)})$ for (18) we solve the following convex problem at the κ-th iteration to generate its next feasible point $(w^{(\kappa+1)},x^{(\kappa+1)},t^{(\kappa+1)},R_l^{(\kappa+1)},r_u^{(\kappa+1)})$:

$$\begin{aligned}\max_{\substack{\boldsymbol{w},\mathbf{R},\mathbf{r},\boldsymbol{x},\boldsymbol{t},\\ \boldsymbol{\eta}\triangleq\{\boldsymbol{\eta}_{ik}\ :\ (i,k)\in\mathcal{M}^2\}}}\quad & \Phi^{(\kappa)}(\mathbf{R},\mathbf{r},\boldsymbol{t}_1)\\ \text{s.t.}\quad & (18b)-(18e),(24),(29),(31),(34),(36),(37).\end{aligned} \tag{38}$$

The computational complexity of (38) is

$$\mathcal{O}(n^2m^{2.5}+m^{3.5}), \tag{39}$$

with $n=MN_t+M^2+2M+2$, which is the number of decision variables, and $m=2M^2+7M+1$, which is the number of constraints.

According to [16], $\mathbf{R}_i$ and $\mathbf{r}_{ik}$ are the root of $\zeta_i(w^{(\kappa+1)},\mathbf{R}_i)=0$ and $g_{ik}(\mathbf{r}_{ik},w^{(\kappa+1)},x^{(\kappa+1)},t_2^{(\kappa+1)})=0$, respectively. At the same κ-th iteration, $R_i^{(\kappa+1)}$, $i\in\mathcal{M}$ and $r_{ik}^{(\kappa+1)}$, $(i,k)\in\mathcal{M}\times\mathcal{M}$ are then found from solving the following nonlinear equations by bisection

$$\begin{aligned}\zeta_i(w^{(\kappa+1)},\mathbf{R}_i)=&-\varphi_i(w^{(\kappa+1)},\mathbf{R}_i)+\delta\frac{M-1}{2}n_{\min}(w^{(\kappa+1)})\\ &\times\ln\frac{\varphi_i(w^{(\kappa+1)},\mathbf{R}_i)}{n_{\min}(w^{(\kappa+1)})}+\delta\delta_M n_{\min}(w^{(\kappa+1)})\\ =&\ 0,\end{aligned} \tag{40}$$

and

$$g_{ik}(\mathbf{r}_{ik},w^{(\kappa+1)},x^{(\kappa+1)},t_2^{(\kappa+1)})=0. \tag{41}$$

Note that the convex problem (38) is an inner approximation of the nonconvex problem (18) in the sense that any feasible point for the former is also feasible point for the latter. As $(w^{(\kappa)},x^{(\kappa)},t^{(\kappa)},R^{(\kappa)},r^{(\kappa)})$ and $(w^{(\kappa+1)},x^{(\kappa+1)},t^{(\kappa+1)},R_l^{(\kappa+1)},r_u^{(\kappa+1)})$ are a feasible point and the optimal solution of (38), we have

$$\begin{aligned}\Phi^{(\kappa)}(R^{(\kappa+1)},r^{(\kappa+1)},t_1^{(\kappa+1)}) \quad &> \quad \Phi^{(\kappa)}(R^{(\kappa)},r^{(\kappa)},t_1^{(\kappa)})\\ &= \quad \Phi(R^{(\kappa)},r^{(\kappa)},t_1^{(\kappa)})\end{aligned} \tag{42}$$

as far as

$$\begin{aligned}&(w^{(\kappa)},x^{(\kappa)},t^{(\kappa)},R^{(\kappa)},r^{(\kappa)}) \quad \neq\\ &(w^{(\kappa+1)},x^{(\kappa+1)},t^{(\kappa+1)},R_l^{(\kappa+1)},r_u^{(\kappa+1)}).\end{aligned}$$

By (21)

$$\Phi(R^{(\kappa+1)},r^{(\kappa+1)},t_1^{(\kappa+1)})\geq\Phi^{(\kappa)}(R^{(\kappa+1)},r^{(\kappa+1)},t_1^{(\kappa+1)})$$

which together with (42) imply

$$\Phi(R^{(\kappa+1)},r^{(\kappa+1)},t_1^{(\kappa+1)})>\Phi(R^{(\kappa)},r^{(\kappa)},t_1^{(\kappa)}), \tag{43}$$

i.e. $(w^{(\kappa+1)},x^{(\kappa+1)},t^{(\kappa+1)},R^{(\kappa+1)},r^{(\kappa+1)})$ is a better feasible point for (18) than $(w^{(\kappa)},x^{(\kappa)},t^{(\kappa)},R^{(\kappa)},r^{(\kappa)})$. As such the sequence $\{(w^{(\kappa)},x^{(\kappa)},t^{(\kappa)},R^{(\kappa)},r^{(\kappa)})\}$ of improved feasible points for (18) converges at least to its locally optimal solution [29].

An initial feasible point $(w^{(0)},x^{(0)},t^{(0)},R^{(0)},r^{(0)})$ can be easily found by taking any $(w^{(0)},x^{(0)},t^{(0)})$ feasible for the convex constraints (18b) and (18d) and then solving the nonlinear equations (40) and (41) with $(w^{(\kappa+1)},x^{(\kappa+1)})$ replaced by $(w^{(0)},x^{(0)})$ for $R_i^{(0)}$ and $r_{ik}^{(0)}$.

Algorithm 1 provides the pseudo-code for computing (18).

It is noteworthy that setting $1/\boldsymbol{t}_1=1$ (so $1/\boldsymbol{t}_2=0$) in the proposed time-fraction based transmission leads to the conventional time-slot transmission as in [17]. Our simulations will particularly compare the performance of these two transmissions.

Algorithm 1 Path-following algorithm for MISO maximin secrecy rate optimization

Initialization: Set $\kappa = 0$. Take an initial feasible point $(w^{(0)}, x^{(0)}, t^{(0)}, R^{(0)}, r^{(0)})$ for (18).

Repeat until convergence of the objective function in (18): Solve the convex problem (38) to obtain the feasible point $(w^{(\kappa+1)}, R_l^{(\kappa+1)}, r_u^{(\kappa+1)}, x^{(\kappa+1)}, t^{(\kappa+1)})$ for (18); Solve the nonlinear equations (40) and (41) to obtain the roots $R_i^{(\kappa+1)}$ and $r_i^{(\kappa+1)}$; Reset $\kappa \leftarrow \kappa + 1$.

1) Special case of SISO interference network: We now consider a particular single-input single-output (SISO) case when each TR j is equipped with a single antenna to exploit the results of [16] tailored for SISO networks. Accordingly, the equation (1) for the signal received at UE i during the time-fraction $1/\boldsymbol{t}_1$ is specified to

$$y_i = \sqrt{h_{ii}}\sqrt{\mathbf{p}_i}s_i + \sum_{j\neq i}^{M}\sqrt{h_{ji}}\sqrt{\mathbf{p}_j}s_j + n_i, i \in \mathcal{M}, \quad (44)$$

where $h_{ji} > 0$ is the channel gain from TR j to UE i, $\sqrt{\mathbf{p}_j}$ is the power allocated to the information symbol s_j, and $n_i \in \mathcal{CN}(0, \sigma^2\mathcal{B})$ is white Gaussian background noise as in (1). The channel gain is modelled by

$$h_{ji} = \bar{h}_{ji}(1 + \delta\chi_{ji}), \quad (45)$$

where $\bar{h}_{ji} > 0$ and $0 < \delta \ll 1$ are deterministic, and $\chi_{ij} \in \mathcal{CN}(0, 1)$. Thus, $\bar{h}_{ij}$ represents the channel gain' estimation and $\delta\chi_{ij}$ represents the estimation quality. Another case of $h_{ji} = \bar{h}_{ji}\chi_{ji}$ was considered in [30].

The equations (3) and (4) for the signals received at EV k during the time-fraction $1/\boldsymbol{t}_1$ and $1/\boldsymbol{t}_2$ are

$$y_{1k}^E = \sum_{i=1}^{M}\sqrt{h_{ik,e}}\sqrt{\mathbf{p}_i}s_i + n_e, \quad (46)$$

and

$$y_{2k}^E = \sum_{i=1}^{M}\sqrt{h_{ik,e}}\Delta_i + n_e, \quad (47)$$

where $h_{ik,e} > 0$ is the channel gain from TR i to UE k, $\Delta_i \in \mathcal{CN}(0, \boldsymbol{x}_i^2)$ is AN of the power $\boldsymbol{x}_i^2$, and $n_e \in \mathcal{CN}(0, \sigma^2\mathcal{B})$ is white Gaussian background noise as in (3) and (4). The channel gain $h_{ik,e}$ from TR i to EV k is now modeled by

$$h_{ik,e} = \beta_{ik,e}\chi_{ik}^E \quad (48)$$

with the deterministic $\beta_{ik,e}$ and the random $\chi_{ik}^E \in \mathcal{CN}(0, 1)$.

Let $\mathbf{p} \triangleq \{\mathbf{p}_i : i \in \mathcal{M}\}$ and $\boldsymbol{x} \triangleq \{\boldsymbol{x}_i : i \in \mathcal{M}\}$. According to [16], UE i' rate is defined by

$$\frac{1}{\boldsymbol{t}_1} \times \max_{\mathbf{R}_i \geq 0} \ln(1 + \mathbf{R}_i) \quad \text{s.t.} \quad f_i(\mathbf{R}_i, \mathbf{p}) \leq 0, \quad (49)$$

for

$$f_i(\mathbf{R}_i, \mathbf{p}) \triangleq \mathbf{p}_i\bar{h}_{ii}[\delta\ln(1-\epsilon) - 1] + \mathbf{R}_i(\sigma_i^2 + \sum_{j\neq i}^{M}\bar{h}_{ji}\mathbf{p}_j) + \delta\bar{h}_{ii}\mathbf{p}_i\sum_{j\neq i}^{M}\ln\left(1 + \frac{\bar{h}_{ji}\mathbf{R}_i\mathbf{p}_j}{\bar{h}_{ii}\mathbf{p}_i}\right), \quad (50)$$

while EV k's rate of overhearing s_i by treating y_{1k}^E in (46) as noise is defined by

$$\max_{\mathbf{r}_{ik}\geq 0} \ln(1 + \mathbf{r}_{ik}) \quad \text{s.t.} \quad \tilde{g}_{ik}(\mathbf{r}_{ik}, \mathbf{p}, \boldsymbol{x}, \boldsymbol{t}_2) \geq 0, \quad (51)$$

for

$$\tilde{g}_{ik}(\mathbf{r}_{ik}, \mathbf{p}, \boldsymbol{x}, \boldsymbol{t}_2) \triangleq \bar{h}_{ik,e}\ln(1-\epsilon_{EV}) + \left(\frac{1}{\boldsymbol{t}_2}\sum_{i=1}^{M}\bar{h}_{ik,e}\boldsymbol{x}_i^2 + \sigma_e^2\right)\frac{\mathbf{r}_{ik}}{\mathbf{p}_i} + \bar{h}_{ik,e}\sum_{j\neq i}^{M}\ln\left(1 + \frac{\mathbf{r}_{ik}\bar{h}_{jk,e}\mathbf{p}_j}{\bar{h}_{ik,e}\mathbf{p}_i}\right). \quad (52)$$

With the function $\varphi_i(\mathbf{R}_i, \mathbf{r}_i, \boldsymbol{t}_1)$ defined from (15), the problem is max-min secrecy rate optimization is formulated as

$$\max_{\mathbf{p},\boldsymbol{x},\boldsymbol{t},\mathbf{R},\mathbf{r}} \Phi(\mathbf{R}, \mathbf{r}, \boldsymbol{t}_1) \triangleq \min_{i\in\mathcal{M}} \varphi_i(\mathbf{R}_i, \mathbf{r}_i, \boldsymbol{t}_1)$$

$$\text{s.t.} \quad (18\text{d}), (18\text{e}), \quad (53a)$$

$$\frac{\mathbf{p}_i}{\boldsymbol{t}_1} + \frac{\boldsymbol{x}_i^2}{\boldsymbol{t}_2} \leq P_i, i \in \mathcal{M}, \quad (53b)$$

$$\mathbf{p}_i \leq 3P_i, \boldsymbol{x}_i^2 \leq 3P_i, i \in \mathcal{M}, \quad (53c)$$

$$f_i(\mathbf{R}_i, \mathbf{p}) \leq 0, i \in \mathcal{M}, \quad (53d)$$

$$\tilde{g}_{ik}(\mathbf{r}_{ik}, \mathbf{p}, \boldsymbol{x}, \boldsymbol{t}_2) \geq 0, i \in \mathcal{M}, k \in \mathcal{M}, \quad (53e)$$

which is a nonconvex problem because the objective in (53a) is nonconcave, while the constraints (53b), (53d) and (53e) are nonconvex.

Let $(p^{(\kappa)}, x^{(\kappa)}, t^{(\kappa)}, R^{(\kappa)}, r^{(\kappa)})$ be a feasible point for (52) found from the $(\kappa-1)$-th iteration. Note that [16, (76)]

$$\mathbf{p}_i \leq 0.5(\mathbf{p}_i^2/p_i^{(\kappa)} + p_i^{(\kappa)})$$

that yields

$$\frac{\mathbf{p}_i}{\boldsymbol{t}_1} + \frac{\boldsymbol{x}_i^2}{\boldsymbol{t}_2} \leq 0.5\frac{\mathbf{p}_i^2/p_i^{(\kappa)} + p_i^{(\kappa)}}{\boldsymbol{t}_1} + \frac{\boldsymbol{x}_i^2}{\boldsymbol{t}_2}.$$

Since the right hand side (RHS) of the last inequality is a convex function, the nonconvex constraint (53b) is innerly approximated by the following convex constraint

$$0.5\frac{\mathbf{p}_i^2/p_i^{(\kappa)} + p_i^{(\kappa)}}{\boldsymbol{t}_1} + \frac{\boldsymbol{x}_i^2}{\boldsymbol{t}_2} \leq P_i, i \in \mathcal{M}. \quad (54)$$

To handle the nonconvex constraint (53d) with $f_i(\mathbf{R}_i, \mathbf{p})$ defined from (50), we first apply the inequality (79) in the appendix for $z = \bar{h}_{ji}\mathbf{R}_i\mathbf{p}_j/(\bar{h}_{ii}\mathbf{p}_i)$ and $\bar{z} = \bar{h}_{ji}R_i^{(\kappa)}p_j^{(\kappa)}/(\bar{h}_{ii}p_i^{(\kappa)})$ and then use the following inequality

$$\mathbf{R}_i\mathbf{p}_j \leq \upsilon_{ij}^{(\kappa)}(\mathbf{R}_i, \mathbf{p}_j) \triangleq \frac{R_i^{(\kappa)}p_j^{(\kappa)}}{4}(\frac{\mathbf{R}_i}{R_i^{(\kappa)}} + \frac{\mathbf{p}_j}{p_j^{(\kappa)}})^2 \quad (55)$$

to obtain

$$\mathbf{p}_i\ln\left(1 + \frac{\bar{h}_{ji}\mathbf{R}_i\mathbf{p}_j}{\bar{h}_{ii}\mathbf{p}_i}\right) \leq \mathbf{p}_i\left[\ln\left(1 + \frac{\bar{h}_{ji}R_i^{(\kappa)}p_j^{(\kappa)}}{\bar{h}_{ii}p_i^{(\kappa)}}\right)\right.$$

$$+\frac{1}{\frac{\bar{h}_{ii}}{\bar{h}_{ji}}+\frac{R_i^{(\kappa)}p_j^{(\kappa)}}{p_i^{(\kappa)}}}\left(\frac{\mathbf{R}_i\mathbf{p}_j}{\mathbf{p}_i}-\frac{R_i^{(\kappa)}p_j^{(\kappa)}}{p_i^{(\kappa)}}\right)\Bigg] \leq \mathbf{p}_i\ln\left(1+\frac{\bar{h}_{ji}R_i^{(\kappa)}p_j^{(\kappa)}}{\bar{h}_{ii}p_i^{(\kappa)}}\right)$$
$$+\frac{1}{\frac{\bar{h}_{ii}}{\bar{h}_{ji}}+\frac{R_i^{(\kappa)}p_j^{(\kappa)}}{p_i^{(\kappa)}}}\left(\upsilon_{ij}^{(\kappa)}(\mathbf{R}_i,\mathbf{p}_j)-\frac{R_i^{(\kappa)}p_j^{(\kappa)}}{p_i^{(\kappa)}}\mathbf{p}_i\right) \triangleq \Phi_{ij}^{(\kappa)}(\mathbf{R}_i,\mathbf{p}_i,\mathbf{p}_j) \quad (56)$$

that yields

$$f_i(\mathbf{R}_i,\mathbf{p}) \leq \mathbf{p}_i\bar{h}_{ii}[\delta\ln(1-\epsilon)-1]+\sigma_i^2\mathbf{R}_i+\sum_{j\neq i}^{M}\bar{h}_{ji} \times \upsilon_{ij}^{(\kappa)}(\mathbf{R}_i,\mathbf{p}_j)+\delta\bar{h}_{ii}\sum_{j\neq i}^{M}\Phi_{ij}^{(\kappa)}(\mathbf{R}_i,\mathbf{p}_i,\mathbf{p}_j) \triangleq f_i^{(\kappa)}(\mathbf{R}_i,\mathbf{p}). \quad (57)$$

Consequently, the nonconvex constraint (53d) is innerly approximated by the following convex constraint

$$f_i^{(\kappa)}(\mathbf{R}_i,\mathbf{p}) \leq 0. \quad (58)$$

To handle the nonconvex constraint (53e), by applying the inequality (83) in the appendix for $z=\bar{h}_{jk,e}\mathbf{r}_{ik}\mathbf{p}_j$, $\tau=\bar{h}_{ik,e}\mathbf{p}_i$ and $\bar{z}=\bar{h}_{jk,e}r_{ik}^{(\kappa)}p_j^{(\kappa)}$, $\bar{\tau}=\bar{h}_{ik,e}p_i^{(\kappa)}$, we obtain

$$\ln\left(1+\frac{\bar{h}_{jk,e}\mathbf{r}_{ik}\mathbf{p}_j}{\bar{h}_{ik,e}\mathbf{p}_i}\right) \geq \ln(1+\chi_{ijk}^{(\kappa)}) + \xi_{ijk}^{(\kappa)}\left(2-\frac{r_{ik}^{(\kappa)}p_j^{(\kappa)}}{\mathbf{r}_{ik}\mathbf{p}_j}-\frac{\mathbf{p}_i}{p_i^{(\kappa)}}\right) \triangleq \lambda_{ijk}^{(\kappa)}(\mathbf{r}_{ik},\mathbf{p}_j,\mathbf{p}_i), \quad (59)$$

with $\chi_{ijk}^{(\kappa)} \triangleq r_{ik}^{(\kappa)}\bar{h}_{jk,e}p_j^{(\kappa)}/\bar{h}_{ik,e}p_i^{(\kappa)}$ and $\xi_{ijk}^{(\kappa)} \triangleq \chi_{ijk}^{(\kappa)}/(\chi_{ijk}^{(\kappa)}+1)$. By introducing the scalar variables $\boldsymbol{\eta}_{ik}$, $i\in\mathcal{M}$, $k\in\mathcal{M}$, satisfying the constraint

$$\left(\frac{1}{\boldsymbol{t}_2}\sum_{i=1}^{M}\bar{h}_{ik,e}\boldsymbol{x}_i^2+\sigma_e^2\right)\frac{\mathbf{r}_{ik}}{\mathbf{p}_i} \geq \boldsymbol{\eta}_{ik}, i\in\mathcal{M}, k\in\mathcal{M}, \quad (60)$$

the nonconvex constraint (53e) is innerly approximated by the convex constraint

$$\bar{h}_{ik,e}\ln(1-\epsilon_{EV})+\boldsymbol{\eta}_{ik}+\bar{h}_{ik,e}\sum_{j\neq i}^{M}\lambda_{ijk}^{(\kappa)}(\mathbf{r}_{ik},\mathbf{p}_j,\mathbf{p}_i) \geq 0, \quad i\in\mathcal{M}, k\in\mathcal{M}. \quad (61)$$

As (60) is a nonconvex constraint, we need to provide its inner convex approximation. Note that

$$(60) \Leftrightarrow \sum_{i=1}^{M}\bar{h}_{ik,e}\frac{\boldsymbol{x}_i^2}{\boldsymbol{t}_2}+\sigma_e^2 \geq \frac{\boldsymbol{\eta}_{ik}\mathbf{p}_i}{\mathbf{r}_{ik}}, i\in\mathcal{M}, k\in\mathcal{M}, \quad (62)$$

which is innerly approximated by the following convex constraint

$$\sum_{i=1}^{M}\bar{h}_{ik,e}\left(\frac{2x_i^{(\kappa)}}{t_2^{(\kappa)}}\boldsymbol{x}_i-\frac{(x_i^{(\kappa)})^2}{(t_2^{(\kappa)})^2}\boldsymbol{t}_2\right)+\sigma_e^2 \geq \frac{\eta_{ik}^{(\kappa)}p_i^{(\kappa)}}{4\mathbf{r}_{ik}}(\frac{\boldsymbol{\eta}_{ik}}{\eta_{ik}^{(\kappa)}}+\frac{\mathbf{p}_i}{p_i^{(\kappa)}})^2, i\in\mathcal{M}, k\in\mathcal{M}. \quad (63)$$

Thus the nonconvex constraint (53e) is innerly approximated by the convex constraints (61) and (63).

Initialized from a feasible point $(p^{(0)},x^{(0)},t^{(0)},R^{(0)},r^{(0)})$ for the nonconvex problem (53) we solve the following convex problem of inner approximation of (53) at the κ-th iteration to generate its next feasible point $(p^{(\kappa+1)},x^{(\kappa+1)},t^{(\kappa+1)},R_l^{(\kappa+1)},r_u^{(\kappa+1)})$:

$$\max_{\mathbf{p},\boldsymbol{x},\boldsymbol{t},\mathbf{R},\mathbf{r},\boldsymbol{\eta}\triangleq\{\boldsymbol{\eta}_{ik}\,:\,(i,k)\in\mathcal{M}^2\}} \Phi^{(\kappa)}(\mathbf{R},\mathbf{r},\boldsymbol{t}_1)$$
$$\text{s.t.} \quad (18\text{d}),(18\text{e}),(53\text{c}),(54),(58),(61),(63), \quad (64)$$

where $\Phi^{(\kappa)}(\mathbf{R},\mathbf{r},\boldsymbol{t}_1)$ is defined by (21), which is a concave lower bounding approximation of the objective function $\Phi(\mathbf{R},\mathbf{r},\boldsymbol{t}_1)$ in (53). The computational complexity of (64) is (39) with $n=M^2+3M+2$, which is the number of decision variables, and $m=2M^2+5M+1$, which is the number of constraints.

At the same $k-$th iteration, $R_i^{(\kappa+1)}$, $i\in\mathcal{M}$, and $r_{ik}^{(\kappa+1)}$, $(i,k)\in\mathcal{M}\times\mathcal{M}$, are found from solving the following nonlinear equations by bisection

$$f_i(\mathbf{R}_i,p^{(\kappa+1)})=0, \quad (65)$$

and

$$\tilde{g}_{ik}(\mathbf{r}_{ik},p^{(\kappa+1)},x^{(\kappa+1)},t_2^{(\kappa+1)})=0. \quad (66)$$

Similar to (43), we can show that

$$\Phi(R^{(\kappa+1)},r^{(\kappa+1)},t_1^{(\kappa+1)}) > \Phi(R^{(\kappa)},r^{(\kappa)},t_1^{(\kappa)}) \quad (67)$$

as far as $(p^{(\kappa+1)},x^{(\kappa+1)},t^{(\kappa+1)},R^{(\kappa+1)},r^{(\kappa+1)}) \neq (p^{(\kappa)},x^{(\kappa)},t^{(\kappa)},R^{(\kappa)},r^{(\kappa)})$, i.e. the former is a better feasible point for (53) than the latter, so Algorithm 2 converges at least to a locally optimal solution of (53).

An initial feasible point $(p^{(0)},x^{(0)},t^{(0)},R^{(0)},r^{(0)})$ for (53) can be easily located by taking any $t^{(0)} \triangleq (t_1^{(0)},t_2^{(0)})$ satisfying the convex constraint (18d) and then $(p^{(0)},x^{(0)})$ satisfying the convex constraint (53b) with $\boldsymbol{t}$ held fixed at $t^{(0)}$, and then solving the nonlinear equations (65) and (66) with $(p^{(\kappa+1)},x^{(\kappa+1)},t_2^{(\kappa+1)})$ replaced by $(p^{(0)},x^{(0)},t_2^{(0)})$.

Algorithm 2 Path-following algorithm for SISO maximin secrecy rate optimization

Initialization: Set $\kappa=0$. Choose an initial feasible point $(p^{(0)},x^{(0)},t^{(0)},R^{(0)},r^{(0)})$ for (53).

Repeat until convergence of the objective function in (53): Solve the convex problem (64) to obtain the solution $(p^{(\kappa+1)},x^{(\kappa+1)},t^{(\kappa+1)},R_l^{(\kappa+1)},r_u^{(\kappa+1)})$; Solve the nonlinear equations (65) and (66) for $R_i^{(\kappa+1)}$ and $r_{ik}^{(\kappa+1)}$; Reset $\kappa\leftarrow\kappa+1$.

III. Secure FBL regime

We consider the equations (1), (3), and (4) for the signals received at UE i during the time-fraction $1/\boldsymbol{t}_1$, at EV k during the time-fractions $1/\boldsymbol{t}_1$ and $1/\boldsymbol{t}_2$, under the channel conditions defined by (2) and (5) in the FBL regime. Based on the

definition (15) for UE i' secrecy rate in the LBL regime, and [20, (106)] for the achievable secrecy rate for the error probability constrained by ϵ^c and the total variation secrecy constrained by ϵ^v for additional white Gaussian noise (AWGN) channels, we propose the following function for approximating UE i' secrecy rate under FBL[5]

$$\tilde{\varphi}_i(\mathbf{R}_i,\mathbf{r}_i,\boldsymbol{t}_1) \triangleq (\rho_i(\mathbf{R}_i,\boldsymbol{t}_1) - a^c\tilde{\rho}_i(\mathbf{R}_i,\boldsymbol{t}_1)) - \max_{k\in\mathcal{M}}\left(\rho_{E,ik}(\mathbf{r}_{ik}) + a^v\tilde{\rho}_{E,ik}(\mathbf{r}_{ik})\right), \quad (68)$$

where $a^c \triangleq Q_G^{-1}(\epsilon^c)/\sqrt{\tau\mathcal{B}}$ and $a^v \triangleq Q_G^{-1}(\epsilon^v)/\sqrt{\tau\mathcal{B}}$, τ is the transmission duration, and $Q_G^{-1}(.)$ is the inverse of the Gaussian Q-function $Q(z) = \int_z^\infty \frac{1}{\sqrt{2\pi}}\exp(-\bar{z}^2/2)d\bar{z}$, while $\rho_{E,ik}(\mathbf{r}_{ik})$ are defined from (16) and (17), respectively, and

$$\tilde{\rho}_i(\mathbf{R}_i,\boldsymbol{t}_1) \triangleq \frac{1}{\boldsymbol{t}_1}\sqrt{1-\frac{1}{(1+\mathbf{R}_i)^2}} \quad (69)$$

and

$$\tilde{\rho}_{E,ik}(\mathbf{r}_{ik}) = \sqrt{1-\frac{1}{(1+\mathbf{r}_{ik})^2}}. \quad (70)$$

In correspondence with the problem (18) in the LBL regime, we propose the following problem for UEs' max-min secrecy rate optimization in the FBL regime

$$\max_{\boldsymbol{w},\mathbf{R},\mathbf{r},\boldsymbol{x},\boldsymbol{t}} \tilde{\Phi}(\mathbf{R},\mathbf{r},\boldsymbol{t}_1) \triangleq \min_{i\in\mathcal{M}} \tilde{\varphi}_i(\mathbf{R}_i,\mathbf{r}_i,\boldsymbol{t}_1) \quad \text{s.t.} \quad (18b)-(18h), \quad (71)$$

which is obviously seen as a nonconvex problem. As its nonconvex constraints (18f), (18g) and (18h) are innerly approximated by the convex constraints (24), (29), (31), (34), (36), and (37), it remains to handle its nonconcave objective. To this end, we need to approximate the objective function in (71) by a lower-bounding concave function, which requires to find a lower bounding concave function approximation of $\rho_i(\mathbf{R}_i,\boldsymbol{t}_1)$ and find upper bounding convex function approximations for $\rho_{E,ik}(\mathbf{r}_{ik})$, $\tilde{\rho}_i(\mathbf{R}_i,\boldsymbol{t}_1)$, and $\tilde{\rho}_{E,ik}(\mathbf{r}_{ik})$. The lower bounding concave function approximation of $\rho_i(\mathbf{R}_i,\boldsymbol{t}_1)$ is derived in (19), while the upper bounding convex function approximation of $\rho_{E,ik}(\mathbf{r}_{ik})$ is found in (20). Thus, it remains to find the upper bounding convex functions of $\tilde{\rho}_i(\mathbf{R}_i,\boldsymbol{t}_1)$ and $\tilde{\rho}_{E,ik}(\mathbf{r}_{ik})$, which are derived in the following.

Eq. (68) is the nonconcave objective in the problem (71), which should be approximated by a lower-bounding concave function. Specifically, $\rho_i(\mathbf{R}_i,\boldsymbol{t}_1)$ is lower bounded by a concave function $\rho_i^{(\kappa)}(\mathbf{R}_i,\boldsymbol{t}_1)$ in (19), while $\rho_{E,ik}(\mathbf{r}_{ik})$ is upper bounded by a convex function $\rho_{E,ik}^{(\kappa)}(\mathbf{r}_{ik})$ in (20). Then, $\tilde{\rho}_i(\mathbf{R}_i,\boldsymbol{t}_1)$ is upper bounded by a convex function $\tilde{\rho}_i^{(\kappa)}(\mathbf{R}_i,\boldsymbol{t}_1)$ and $\tilde{\rho}_{E,ik}(\mathbf{r}_{ik})$ is upper bounded by a convex function $\tilde{\rho}_{E,ik}^{(\kappa)}(\mathbf{r}_{ik})$. Suppose $(w^{(\kappa)},x^{(\kappa)},t^{(\kappa)},R^{(\kappa)},r^{(\kappa)})$ is a feasible point for (71) found from the $(\kappa-1)$th iteration.

By applying the inequality (80) in the appendix for $z = 1/\boldsymbol{t}_1$, $\tau = 1-1/(1+\mathbf{R}_i)^2$, and $\bar{z} = 1/t_1^{(\kappa)}$, $\bar{\tau} = 1-1/(1+R_i^{(\kappa)})^2$, we obtain

$$\tilde{\rho}_i(\mathbf{R}_i,\boldsymbol{t}_1) = \sqrt{\frac{1}{\boldsymbol{t}_1^2}\left(1-\frac{1}{(1+\mathbf{R}_i)^2}\right)}$$

$$\leq a_i^{(\kappa)} + \frac{b_i^{(\kappa)}}{\boldsymbol{t}_1^2} - \frac{a_i^{(\kappa)}}{(1+\mathbf{R}_i)^2}$$
$$\leq a_i^{(\kappa)} + \frac{b_i^{(\kappa)}}{\boldsymbol{t}_1^2} - \frac{a_i^{(\kappa)}}{2}\left(\frac{3}{(1+R_i^{(\kappa)})^2} - \frac{1+\mathbf{R}_i}{(1+R_i^{(\kappa)})^3}\right)$$
$$\triangleq \tilde{\rho}_i^{(\kappa)}(\mathbf{R}_i,\boldsymbol{t}_1), \quad (72)$$

where

$$0 < a_i^{(\kappa)} = \frac{1}{2t_1^{(\kappa)}\sqrt{1-\frac{1}{(1+R_i^{(\kappa)})^2}}} = \frac{1+R_i^{(\kappa)}}{2t_1^{(\kappa)}\sqrt{(R_i^{(\kappa)})^2+2R_i^{(\kappa)}}},$$
$$b_i^{(\kappa)} = 1/(4a_i^{(\kappa)}), \quad i\in\mathcal{M}.$$

Analogously,

$$\tilde{\rho}_{E,ik}(\mathbf{r}_{ik}) \leq \tilde{\rho}_{E,ik}^{(\kappa)}(\mathbf{r}_{ik}) \triangleq 0.5\left(\tilde{\rho}_{E,ik}(r_{ik}^{(\kappa)}) + \frac{1}{\tilde{\rho}_{E,ik}(r_{ik}^{(\kappa)})}\right) - \frac{1}{4\tilde{\rho}_{E,ik}(r_{ik}^{(\kappa)})}\left(\frac{3}{(1+r_{ik}^{(\kappa)})^2} - \frac{1+\mathbf{r}_{ik}}{(1+r_{ik}^{(\kappa)})^3}\right). \quad (73)$$

Recalling that the function $\rho_i(\mathbf{R}_i,\boldsymbol{t}_1)$ ($\rho_{E,ik}(\mathbf{r}_{ik})$, resp.) in (68) is lower bounded (upper bounded, resp.) by the concave function (convex function, resp.) $\rho_i^{(\kappa)}(\mathbf{R}_i,\boldsymbol{t}_1)$ ($\rho_{E,ik}^{(\kappa)}(\mathbf{r}_{ik})$, resp.) defined by (19) ((20), resp.), the objective function in (71) is thus lower bounded by the following concave function

$$\tilde{\Phi}^{(\kappa)}(\mathbf{R},\mathbf{r},\boldsymbol{t}_1) \triangleq \min_{i\in\mathcal{M}}\left[\rho_i^{(\kappa)}(\mathbf{R}_i,\boldsymbol{t}_1) - a^c\tilde{\rho}_i^{(\kappa)}(\mathbf{R}_i,\boldsymbol{t}_1) - \max_{k\in\mathcal{M}}(\rho_{E,ik}^{(\kappa)}(\mathbf{r}_{ik}) + a^v\tilde{\rho}_{E,ik}^{(\kappa)}(\mathbf{r}_{ik}))\right] \quad (74)$$

Initialized from a feasible point $(w^{(0)},x^{(0)},t^{(0)},R^{(0)},r^{(0)})$ for (71), we solve the following convex problem of its inner approximation to generate the next feasible point $(w^{(\kappa+1)},x^{(\kappa+1)},t^{(\kappa+1)},R_l^{(\kappa+1)},r_u^{(\kappa+1)})$ at the κ-th iteration:

$$\max_{\boldsymbol{w},\mathbf{R},\mathbf{r},\boldsymbol{x},\boldsymbol{t},\boldsymbol{\eta}} \tilde{\Phi}^{(\kappa)}(\mathbf{R},\mathbf{r},\boldsymbol{t}_1)$$
$$\text{s.t} \quad (18b)-(18e),(24),(29),(31),(34),(36),(37). \quad (75)$$

The computational complexity of (75) is (39) with $n = MN_t + M^2 + 2M + 2$, which is the number of its decision variables and $m = 2M^2+7M+1$, which is the number of its constraints.

At the same κ-th iteration, $R_i^{(\kappa+1)}$ and $r_{ik}^{(\kappa+1)}$ are then found from solving the nonlinear equations (40) and (41) by bisection.

An initial feasible point $(w^{(0)},x^{(0)},t^{(0)},R^{(0)},r^{(0)})$ is taken as the optimal solution of (18), which is computed by Algorithm 1. Similar to Algorithm 1, Algorithm 3 generates a sequence $\{(w^{(\kappa)},x^{(\kappa)},t^{(\kappa)},R^{(\kappa)},r^{(\kappa)})\}$ of improved feasible

[5]The interferences in (1) and (4) are well approximated by white Gaussian noise [31].

This article has been accepted for publication in a future issue of this journal, but has not been fully edited. Content may change prior to final publication. Citation information: DOI 10.1109/TIFS.2021.3076927, IEEE Transactions on Information Forensics and Security

Algorithm 3 Path-following algorithm for MISO maximin secrecy rate optimization in FBL regime

Initialization: Set $\kappa = 0$. Choose an initial feasible point $(w^{(0)}, x^{(0)}, t^{(0)}, R^{(0)}, r^{(0)})$ for (71).

Repeat until convergence of the objective function in (71): Solve the convex problem (75) to obtain the feasible point $(w^{(\kappa+1)}, x^{(\kappa+1)}, t^{(\kappa+1)}, R_l^{(\kappa+1)}, r_u^{(\kappa+1)})$ for (71); Solve the nonlinear equations (40) and (41) to obtain the roots $R_i^{(\kappa+1)}$ and $r_i^{(\kappa+1)}$. Reset $\kappa \leftarrow \kappa + 1$.

points for (71), which at least converges to its locally optimal solution.

Analogously, in correspondence with the problem (53) of UEs' max-min secrecy rate optimization under LBL regime for the SISO equations (44), (46), and (47) for the signals received at UE i during the time-fraction $1/\boldsymbol{t}_1$, at EV k during the time-fractions $1/\boldsymbol{t}_1$ and $1/\boldsymbol{t}_2$, under the channel conditions defined by (45) and (48), we propose the following problem for UEs's max-min secrecy rate optimization under FBL regime

$$\max_{\mathbf{p},\boldsymbol{x},\boldsymbol{t},\mathbf{R},\mathbf{r}} \ \tilde{\Phi}(\mathbf{R},\mathbf{r},\boldsymbol{t}_1) \quad \text{s.t.} \quad (18\text{d}), (18\text{e}), (53b) - (53e), \quad (76)$$

where the objective function $\tilde{\Phi}(\mathbf{R},\mathbf{r},\boldsymbol{t}_1)$ is the same as that in (71).

Initialized from its feasible point $(p^{(0)}, x^{(0)}, t^{(0)}, R^{(0)}, r^{(0)})$, we solve the following convex problem of inner approximation of (76) at the κ-th iteration to generate its next feasible point $(p^{(\kappa+1)}, x^{(\kappa+1)}, t^{(\kappa+1)}, R_l^{(\kappa+1)}, r_u^{(\kappa+1)})$ instead of (64):

$$\max_{\mathbf{p},\boldsymbol{x},\boldsymbol{t},\mathbf{R},\mathbf{r},\boldsymbol{\eta}} \ \tilde{\Phi}^{(\kappa)}(\mathbf{R},\mathbf{r},\boldsymbol{t}_1)$$
$$\text{s.t.} \quad (18\text{d}), (18\text{e}), (53\text{c}), (54), (58), (61), (63), \quad (77)$$

with the objective function $\tilde{\Phi}^{(\kappa)}(\mathbf{R},\mathbf{r},\boldsymbol{t}_1)$ defined from (74). At the same k-th iteration, $R_i^{(\kappa+1)}$, $i \in \mathcal{M}$, and $r_{ik}^{(\kappa+1)}$, $(i,k) \in \mathcal{M} \times \mathcal{M}$, are found from solving the nonlinear equations (65) and (66) by bisection.

An initial feasible point $(w^{(0)}, x^{(0)}, t^{(0)}, R^{(0)}, r^{(0)})$ is taken as the optimal solution of (53), which is computed by Algorithm 2. Similar to Algorithm 2, Algorithm 4 generates a sequence $\{(w^{(\kappa)}, x^{(\kappa)}, t^{(\kappa)}, R^{(\kappa)}, r^{(\kappa)})\}$ of improved feasible points for (76), which at least converges to its locally optimal solution.

Algorithm 4 Path-following algorithm for SISO maximin secrecy rate optimization in FBL regime

Initialization: Set $\kappa = 0$. Choose an initial feasible point $(w^{(0)}, x^{(0)}, t^{(0)}, R^{(0)}, r^{(0)})$ for (76).

Repeat until convergence of the objective function in (76): Solve the convex problem (77) to obtain the feasible point $(w^{(\kappa+1)}, x^{(\kappa+1)}, t^{(\kappa+1)}, R_l^{(\kappa+1)}, r_u^{(\kappa+1)})$ for (71); Solve the nonlinear equations (65) and (66) for $R_i^{(\kappa+1)}$ and $r_{ik}^{(\kappa+1)}$; Reset $\kappa \leftarrow \kappa + 1$.

IV. Numerical Examples

This section presents numerical results to demonstrate the efficiency of the proposed schemes. There are $M = 4$ TR-UE pairs and each TR is equipped with $N_t = 4$ antennas. The large scale fading of the channels in (2) and (3) are given by the following path-loss model (see e.g. [22], [24]):

$$\beta_{ji} = -35.3 - 10\alpha \log_{10}(d_{ji}) \ \ (\text{dB})$$

and

$$\beta_{jk,e} = -35.3 - 10\alpha \log_{10}(d_{jk,e}) \ \ (\text{dB}),$$

where $\alpha = 3.76$ is the path-loss exponent, d_{ji} ($d_{jk,e}$, resp.) denotes the distance between TR j and UE i (EV k, resp.). The small-scale fading ϕ_{ji} of the channels in (2) are generated by independent and identically distributed complex normal random variables of zero mean and unit variance. The transmitters (TRs) are located at $(0,0)$m, $(0,90)$m, $(0,180)$m, and $(0,270)$m. The coordinates of all UEs are $(55,0)$m, $(55,90)$m, $(55,180)$m, and $(55,270)$m, while EVs are in better channel conditions than the UEs as they are located nearer to TRs at the coordinates $(50,0)$m, $(50,90)$m, $(50,180)$m, and $(50,270)$m.

The noise power spectral density is set to $\sigma^2 = -174$ dBm/Hz and the outage probability in (6b) and (13b) is $\epsilon = \epsilon_{EV} = 0.1$. Unless stated otherwise, we set the transmit power budget $P_i = 30$ dBm, the communication bandwidth $\mathcal{B} = 5$ MHz and the transmission duration in FLB regime $\tau = 0.05$ msec.The computation tolerance for terminating all proposed Algorithms is $\epsilon_{\text{tol}} = 10^{-4}$.

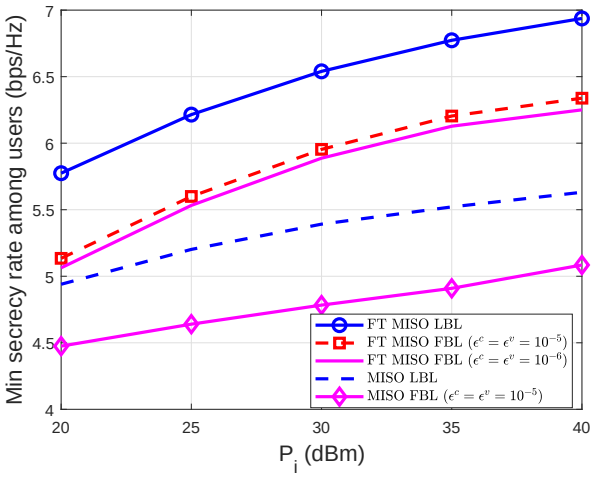

Fig. 2. Minimal secrecy rate among users versus the transmit power limitation P_i.

A. MISO networks

This subsection analyzes the UEs' achievable secrecy rate for MISO systems obtained by four schemes, including "FT MISO LBL" with AN transmission computed by Algorithm 1, "FT MISO FBL" with AN transmission computed by Algorithm 3, "MISO FBL" without AN transmission computed by Algorithm 3 for $\boldsymbol{t}_1 = 1$, and "MISO LBL" without AN transmission computed by an algorithm in [17].

Fig. 2 plots the achievable UEs' minimum secrecy rate versus the transmit power budget P_i. As expected, the secrecy rate increases with the transmit power limitation P_i in all schemes. It is clear from Fig. 2 that "FT MISO LBL" with

This article has been accepted for publication in a future issue of this journal, but has not been fully edited. Content may change prior to final publication. Citation information: DOI 10.1109/TIFS.2021.3076927, IEEE Transactions on Information Forensics and Security

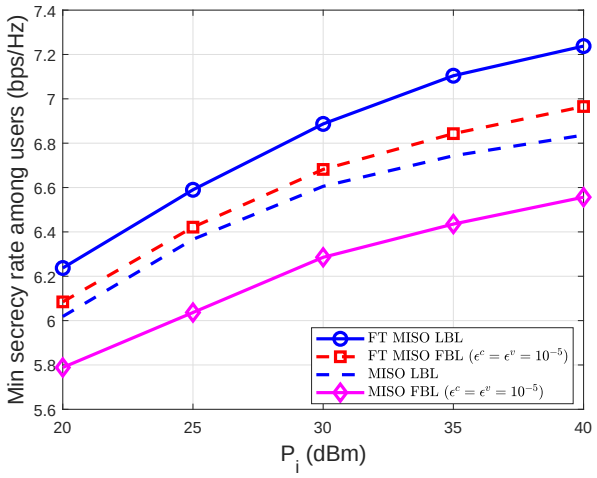

Fig. 3. Minimal secrecy rate among users versus the transmit power limitation P_i in the presence of weaker eavesdropper channels.

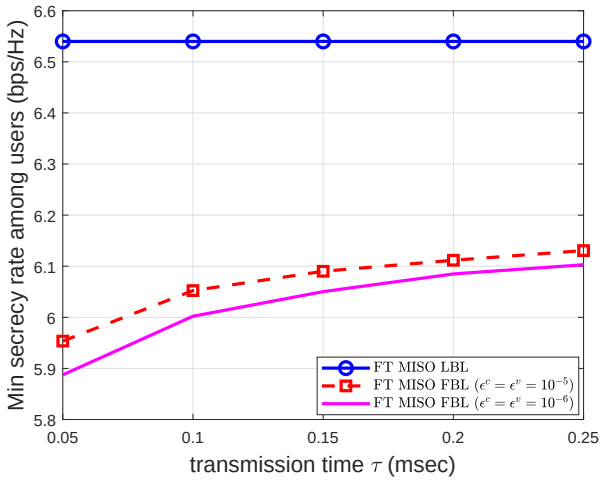

Fig. 4. Minimal secrecy rate among users versus the transmission time τ.

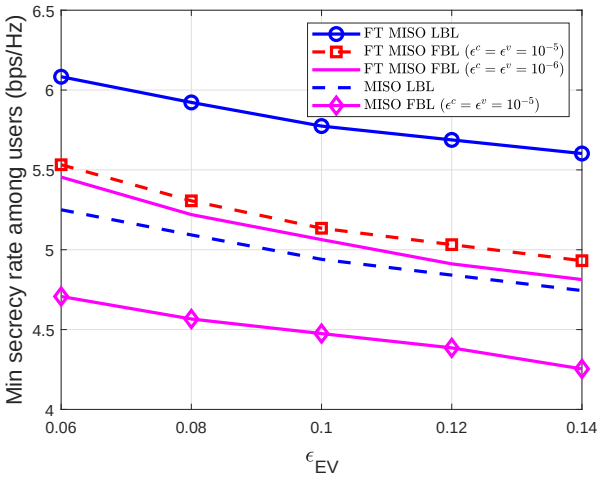

Fig. 5. Minimal secrecy rate among users versus the outage probability ϵ_{EV}.

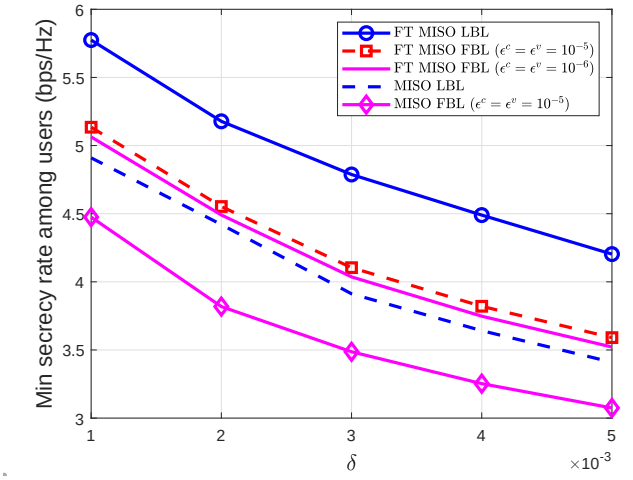

Fig. 6. Minimal secrecy rate among users versus δ.

AN transmission always achieves better secrecy rate than the other schemes. Furthermore, the performance gap between the schemes with AN transmission and that without AN transmission becomes wider with P_i increased. This is because in the presence of multiple strong EVs, the channel gain between the TRs and EVs are stronger than that between the TRs and UEs so it is much harder to control EVs' rate without AN transmission. Fig. 2 also depicts the secrecy rate of "FT MISO FBL" with $\epsilon^c = \epsilon^v = 10^{-5}$ and $\epsilon^c = \epsilon^v = 10^{-6}$), which reveals that the secrecy rate is very sensitive to the FBL error probability ϵ^c and total variation secrecy ϵ^v. The secrecy rate in URLLC deserves more study.

Additionally, we also evaluate the performance of all schemes under weaker eavesdropper channels in Fig. 3 with EVs located at $(60, 0)$m, $(60, 90)$m, $(60, 180)$m, and $(60, 270)$m. The secrecy rate of all schemes increases with the transmit power limitation P_i. Furthermore, the performance gap between the schemes with AN transmission and that without AN transmission is seen narrower than that in the case

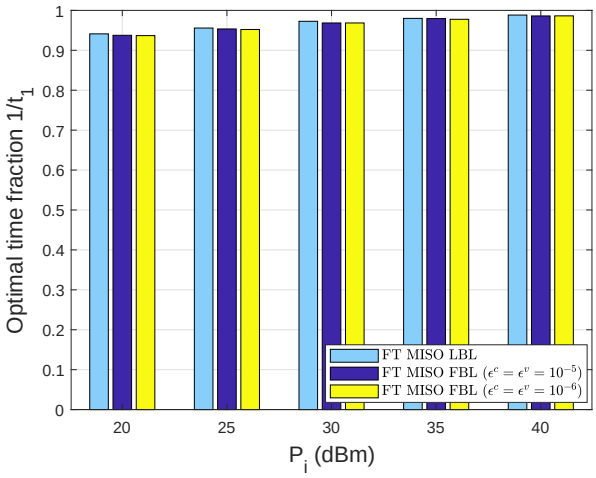

Fig. 7. Optimal fractional-time $1/t_1$ versus the transmit power limitation P_i.

This article has been accepted for publication in a future issue of this journal, but has not been fully edited. Content may change prior to final publication. Citation information: DOI 10.1109/TIFS.2021.3076927, IEEE Transactions on Information Forensics and Security

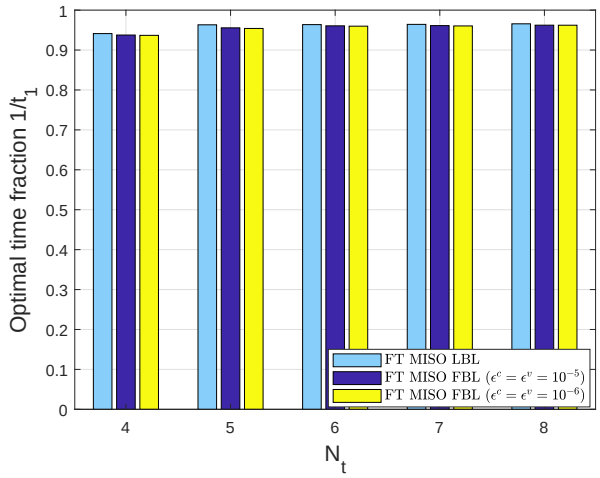

Fig. 8. Optimal fractional-time $1/t_1$ versus the number of transmit antennas N_t.

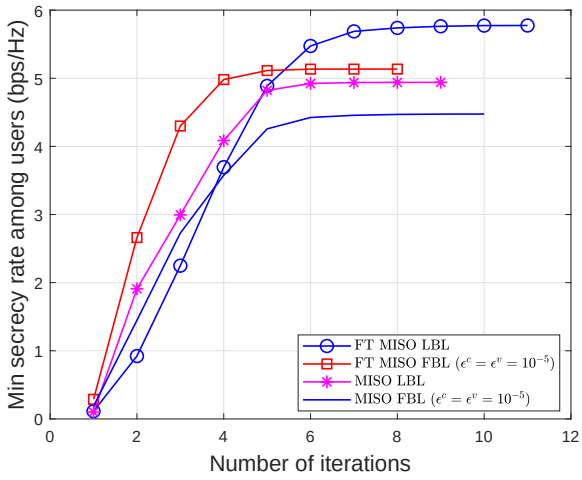

Fig. 9. Convergence of the proposed Algorithms 1 and 3.

of stronger eavesdroppers shown in Fig. 2 because it becomes easier to control the eavesdroppers' rate without AN. From Fig.3, we can still appreciate "FT MISO LBL" and "FT MISO FBL" with AN transmission, which consistently perform better than their counterpart schemes under LBL and FBL regimes, respectively.

Fig. 4 plots the achievable UEs' minimum secrecy rate versus the transmission time τ. As expected, the secrecy rate of "FT MISO FBL" approaches the secrecy rate of "FT MISO LBL" with the increase in the transmission time τ. Fig. 5 plots the achievable UEs' minimum secrecy rate versus the outage probability ϵ_{EV}. It can be observed that the achievable UEs' minimum secrecy rate performance degrades as the outage probability ϵ_{EV} increases. This is because EV k's rate, defined in (13), increases with the increase in outage probability ϵ_{EV}, which decreases the achievable UE's minimum secrecy rate. Additionally, we examine the impact of channel estimation error on the achievable UEs' minimum secrecy rate. It can be observed from Fig. 6 that the achievable UEs' minimum secrecy rate decreases with the increase in δ.

Fig. 7 plots the optimal value of fractional-time $1/t_1$ (for information transmission) versus the transmit power budget P_i. It can be observed that the former increases with the latter increased. This means that under the privilege of a higher transmit power budget, a larger fraction of the time slot is used for information transmission. Fig. 7 also shows that the optimal fractional-time $1/t_1$ under "FT MISO LBL" is larger than that under "FT MISO FBL", which means that "FT MISO LBL" is able to reserve more time for information transmission. Fig. 8 plots the optimal value of fractional-time $1/t_1$ versus the number of transmit antennas N_t. It can be seen that the optimal value of fractional-time $1/t_1$ allocated for information transmission increases with the increase in the number of transmit antennas N_t, but it almost saturates for $N_t \geq 5$ antennas.

Fig. 9 plots the convergence of the proposed Algorithms 1 and 3. We can appreciate that the proposed algorithms converge quickly within $6-8$ iterations. As expected, the achievable rates by "FT MISO FBL" and "MISO FBL" are lower than that by "FT MISO LBL" and "MISO LBL", respectively, and therefore, the former converge quickly than the latter.

B. Results in SISO systems

This subsection examines the UEs' max-min secrecy rates under SISO networks, including "FT SISO LBL" computed by Algorithm 2, "FT SISO FBL" computed by Algorithm 4, "SISO LBL" and "SISO FBL" without AN transmission computed by Algorithm 2 and Algorithm 4 for $\boldsymbol{t}_1 = 1$.

Fig. 10 plots the achievable users' minimum secrecy rate versus the transmit power budget P_i. As expected, the secrecy rate of all schemes increases with the transmit power budget P_i. We also can observe that the secrecy rate of "FT SISO LBL" with AN is always better than that of the other schemes. Observe that in the presence of multiple strong eavesdroppers, the secrecy rate of "SISO FBL" is always negative. The channel gain between the TRs and EVs are stronger than that between the TRs and UEs, which makes the transmission without AN powerless in providing a secure communication to the UEs.

Fig. 11 plots the achievable users' minimum secrecy rate versus the transmission time τ. As expected, the secrecy rate of "FT SISO FBL" approaches the secrecy rate of "FT SISO LBL" with τ increased. Finally, Fig. 12 plots the optimal value of fractional-time $1/t_1$ for information transmission versus the transmit power budget P_i. Under the privilege of a higher transmit power budget, a larger fraction of the time-slot is exploited for information transmission.

V. Conclusions

The paper has considered a physical layer security (PLS) aided wireless interference network of multiple transmitter-user pairs, which is overheard by multiple eavesdroppers (EVs) that have better channel conditions than the legitimate users (UEs). By exploiting information on UEs' and EVs' channel distributions, we have posed the problems of jointly

This article has been accepted for publication in a future issue of this journal, but has not been fully edited. Content may change prior to final publication. Citation information: DOI 10.1109/TIFS.2021.3076927, IEEE Transactions on Information Forensics and Security

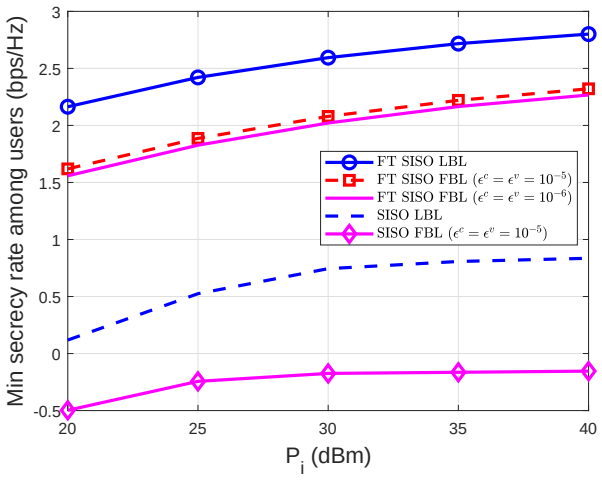

Fig. 10. Minimal secrecy rate among users versus the transmit power limitation P_i for SISO system.

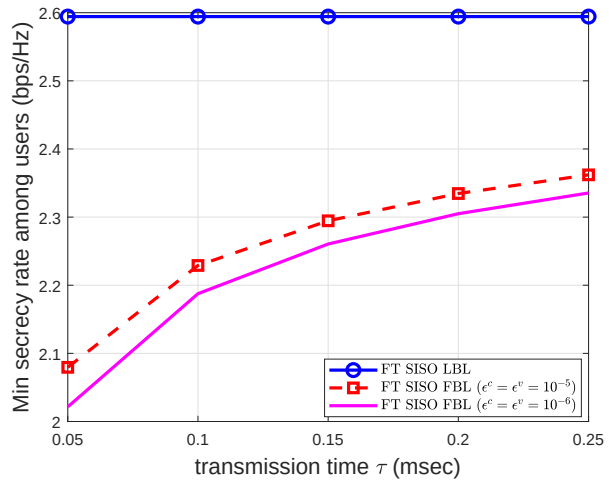

Fig. 11. Minimal secrecy rate among users versus the transmission time τ for SISO system.

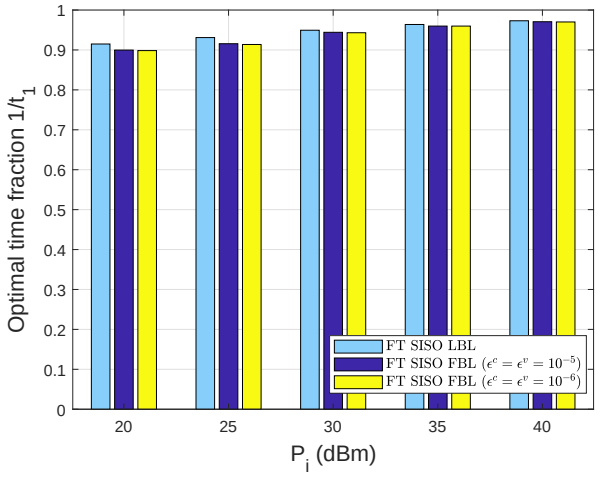

Fig. 12. Optimal time fraction $1/t_1$ versus the transmit power limitation P_i for SISO system.

designing the fractional time-slot allocation for information and artificial noise transmission and transmit beamformers to maximize the UEs' minimum secrecy rate in the both long and short blocklength regimes. Accordingly, we have developed path-following algorithms of low computational complexity and rapid convergence for their computations. Both high performance of the proposed PLS and computational efficiency of the proposed algorithms have been supported by the provided simulations. An extension of this work to broadcasting networks is under current study. One future research direction is to consider multiple antenna at the EVs and design secrecy rate maximization algorithms.

APPENDIX: FUNDAMENTAL INEQUALITIES

We have the following inequalities

$$\ln z \le \ln \bar{z} - 1 + \frac{z}{\bar{z}} \quad \forall\, z > 0, \bar{z} > 0 \tag{78}$$

$$\ln(1+z) \le \ln(1+\bar{z}) + \frac{1}{1+\bar{z}}(z - \bar{z}) \quad \forall\, z \ge 0, \bar{z} \ge 0, \tag{79}$$

$$\sqrt{z\tau} \le \frac{1}{2}\sqrt{\frac{\bar{\tau}}{\bar{z}}}z + \frac{1}{2}\sqrt{\frac{\bar{z}}{\bar{\tau}}}\tau, \tag{80}$$

because their left hand side (LHS) is a concave function while their RHS is the linearization of the LHS at $\bar{z}$ [28]. The following inequalities were proved in [32, Appendix], [18], and [17, (69)]

$$\frac{1}{\tau}\ln(1+z) \ge \frac{2}{\bar{\tau}}\ln(1+\bar{z}) + \frac{\bar{z}}{\bar{\tau}(1+\bar{z})}\left(1 - \frac{\bar{z}}{z}\right) - \frac{\tau}{\bar{\tau}^2}\ln(1+\bar{z}) \forall\, z > 0, \tau > 0, \bar{z} > 0, \bar{\tau} > 0, \tag{81}$$

and

$$\frac{z}{\tau^2} \ge 2\frac{\sqrt{\bar{z}}}{\bar{\tau}^2}\sqrt{z} - \frac{\bar{z}}{\bar{\tau}^4} \quad \forall\, z \ge 0, \tau > 0, \bar{z} \ge 0, \bar{\tau} > 0, \tag{82}$$

and

$$\ln(1+\frac{z}{t}) \ge \ln(1+\frac{\bar{z}}{\bar{t}}) + \frac{\bar{z}}{\bar{z}+\bar{y}}\left(2 - \frac{\bar{z}}{z} - \frac{\tau}{\bar{\tau}}\right) \forall\, z > 0, \tau > 0, \bar{z} > 0, \bar{\tau} > 0. \tag{83}$$

REFERENCES

[1] A. G. Fragkiadakis, E. Z. Tragos, and I. G. Askoxylakis, "A survey on security threats and detection techniques in cognitive radio networks," *IEEE Commun. Surveys Tuts.*, vol. 15, no. 1, pp. 428–445, Jan 2013.

[2] H. V. Poor, "Information and inference in the wireless physical layer," *IEEE Commun. Mag.*, vol. 19, no. 2, pp. 40–47, Feb. 2012.

[3] H. V. Poor and R. F. Schaefer, "Wireless physical layer security," *Proc. Nat. Acad. Sciences USA*, vol. 114, no. 1, pp. 19–26, 2017.

[4] A. Mukherjee, S. A. A. Fakoorian, J. Huang, and A. L. Swindlehurst, "Principles of physical layer security in multiuser wireless networks: A survey," *IEEE Commun. Surveys Tuts.*, vol. 16, no. 3, p. 15501573, Feb 2014.

[5] A. A. Nasir, H. D. Tuan, H. H. Nguyen, and N. M. Nguyen, "Physical layer security by exploiting interference and heterogeneous signaling," *IEEE Wirel. Commun.*, vol. 26, no. 5, pp. 26–31, May 2019.

[6] L. Liu, R. Zhang, and K.-C. Chua, "Secrecy wireless information and power transfer with MISO beamforming," *IEEE Trans. Signal Process.*, vol. 62, no. 4, pp. 1850–1863, Apr. 2014.

[7] N. Nguyen, H. D. Tuan, T. Q. Duong, and H. V. Poor, "MIMO beamforming for secure and energy-efficient wireless communication," *IEEE Signal Process. Lett.*, vol. 24, no. 2, pp. 236–239, Feb. 2017.

[8] A. A. Nasir, H. D. Tuan, T. Q. Duong, and H. V. Poor, "Secrecy rate beamforming for multicell networks with information and energy harvesting," *IEEE Trans. Signal Process.*, vol. 65, no. 3, pp. 677–689, Feb. 2017.

[9] ——, "Secure and energy-efficient beamforming for simultaneous information and energy transfer," *IEEE Trans. Wirel. Commun.*, vol. 16, no. 11, pp. 7523–7537, Nov. 2017.

[10] Q. Li and W. K. Ma, "Spatially selective artificial-noise aided transmit optimization for MISO multi-eves secrecy rate maximization," *IEEE Trans. Signal Process.*, vol. 61, no. 10, pp. 2704–2717, May 2013.

[11] P. Zhao, M. Zhang, H. Yu, H. Luo, and W. Chen, "Robust beamforming design for sum secrecy rate optimization in MU-MISO networks," *IEEE Trans. Info. Forens. Sec.*, vol. 10, no. 9, pp. 1812–1823, Sept. 2015.

[12] Z. Kong, S. Yang, D. Wang, and L. Hanzo, "Robust beamforming and jamming for enhancing the physical layer security of full duplex radios," *IEEE Trans. Info. Forens. Sec.*, vol. 14, no. 12, pp. 3151–3159, 2019.

[13] L. Gui, Y. Zhou, F. Shu, H. Zhou, X. Zhou, J. Li, and J. Wang, "Robust directional modulation design for secrecy rate maximization in multiuser networks," *IEEE Systems Journal*, vol. 14, no. 3, pp. 3150–3160, 2020.

[14] Y. Feng, S. Yan, Z. Yang, N. Yang, and J. Yuan, "Beamforming design and power allocation for secure transmission with NOMA," *IEEE Trans. Wirel. Commun.*, vol. 18, no. 5, pp. 2639–2651, 2019.

[15] D. Hu, P. Mu, W. Zhang, and W. Wang, "Minimization of secrecy outage probability with artificial-noise-aided beamforming for MISO wiretap channels," *IEEE Commun. Lett.*, vol. 24, no. 2, pp. 401–404, 2020.

[16] Z. Sheng, H. D. Tuan, A. A. Nasir, T. Q. Duong, and H. V. Poor, "Power allocation for energy efficiency and secrecy of wireless interference networks," *IEEE Trans. Wirel. Commun.*, vol. 17, no. 6, pp. 3737–3751, Jun. 2018.

[17] Z. Sheng, H. D. Tuan, T. Q. Duong, and H. V. Poor, "Beamforming optimization for physical layer security in MISO wireless networks," *IEEE Trans. Signal Process.*, vol. 66, no. 14, pp. 3710–3723, July 2018.

[18] Z. Sheng, H. D. Tuan, T. Q. Duong, and H. V. Poor, "Outage-aware secure beamforming in MISO wireless interference networks," *IEEE Signal Process. Lett.*, vol. 25, no. 7, pp. 956–960, Jul. 2018.

[19] M. Bennis, M. Debbah, and H. V. Poor, "Ultra-reliable and low-latency wireless communication: Tail, risk, and scale," *Proc. IEEE*, vol. 106, no. 10, pp. 1834–1853, Oct. 2018.

[20] W. Yang, R. F. Schaefer, and H. V. Poor, "Wiretap channels: Nonasymptotic fundamental limits," *IEEE Trans. Inf. Theory*, vol. 65, no. 7, pp. 4069–4093, 2019.

[21] H. Wang, Q. Yang, Z. Ding, and H. V. Poor, "Secure short-packet communications for mission-critical IoT applications," *IEEE Trans. Wirel. Commun.*, vol. 18, no. 5, pp. 2565–2578, 2019.

[22] H. Ren, C. Pan, Y. Deng, M. Elkashlan, and A. Nallanathan, "Resource allocation for secure URLLC in mission-critical IoT scenario," *IEEE Trans. Commun.*, vol. 68, no. 9, pp. 5793–5807, Sept. 2020.

[23] H. H. Kha, H. D. Tuan, and H. H. Nguyen, "Fast global optimal power allocation in wireless networks by local d.c. programming," *IEEE Trans. Wirel. Commun.*, vol. 11, no. 2, pp. 510–515, Feb. 2012.

[24] W. R. Ghanem, V. Jamali, and R. Schober, "Resource allocation for secure multi-user downlink MISO-URLLC systems," in *Proc. of Int. Conf. Commun. (ICC)*, 2020.

[25] A. H. Phan, H. D. Tuan, H. H. Kha, and D. T. Ngo, "Nonsmooth optimization for efficient beamforming in cognitive radio multicast transmission," *IEEE Trans. Signal Process.*, vol. 60, pp. 2941–2951, Jun. 2012.

[26] A. A. Nasir, H. D. Tuan, and T. Q. Duong, "Fractional time exploitation for serving IoT users with guaranteed QoS by 5G spectrum," *IEEE Commun. Mag.*, vol. 56, no. 10, pp. 128–133, Oct. 2018.

[27] B. He, X. Zhou, and A. L. Swindlehurst, "On secrecy metrics for physical layer security over quasi-static fading channels," *IEEE Trans. Wirel. Commun.*, vol. 15, no. 10, pp. 6913–6924, Oct. 2016.

[28] H. Tuy, *Convex Analysis and Global Optimization (second edition)*. Springer International, 2017.

[29] B. R. Marks and G. P. Wright, "A general inner approximation algorithm for nonconvex mathematical programs," *Operation Research*, vol. 26, no. 4, pp. 681–683, 1978.

[30] Z. Sheng, H. D. Tuan, A. A. Nasir, and H. V. Poor, "PLS for wireless interference networks in the short blocklength regime with strong wiretap channels," in *Proc. of Glob. Commun. Conf. (Globecom)*, 2020.

[31] A. A. Nasir, H. D. Tuan, H. H. Nguyen, M. Debbah, and H. V. Poor, "Resource allocation and beamforming design in the short blocklength regime for URLLC," *IEEE Trans. Wirel. Commun.*, vol. 20, no. 2, pp. 1321–1335, Feb. 2020.

[32] Z. Sheng, H. D. Tuan, T. Q. Duong, and H. V. Poor, "Joint power allocation and beamforming for energy-efficient two-way multi-relay communications," *IEEE Trans. Wirel. Commun.*, vol. 16, no. 10, pp. 6660–6671, Jul. 2017.

Zhichao Sheng received the Ph.D. degree in electrical engineering from the University of Technology, Sydney, NSW, Australia in 2018. From 2018 to 2019, he was a Research Fellow at School of Electronics, Electrical Engineering and Computer Science, Queen's University Belfast, Belfast, U.K. He is currently a Lecturer with Shanghai University, Shanghai, China. His research interests include optimization methods for wireless communication and signal processing.

Hoang Duong Tuan received the Diploma (Hons.) and Ph.D. degrees in applied mathematics from Odessa State University, Ukraine, in 1987 and 1991, respectively. He spent nine academic years in Japan as an Assistant Professor in the Department of Electronic-Mechanical Engineering, Nagoya University, from 1994 to 1999, and then as an Associate Professor in the Department of Electrical and Computer Engineering, Toyota Technological Institute, Nagoya, from 1999 to 2003. He was a Professor with the School of Electrical Engineering and Telecommunications, University of New South Wales, from 2003 to 2011. He is currently a Professor with the School of Electrical and Data Engineering, University of Technology Sydney. He has been involved in research with the areas of optimization, control, signal processing, wireless communication, and biomedical engineering for more than 20 years.

Ali Arshad Nasir (S'09-M'13) is an Assistant Professor in the Department of Electrical Engineering, King Fahd University of Petroleum and Minerals (KFUPM), Dhahran, KSA. Previously, he held the position of Assistant Professor in the School of Electrical Engineering and Computer Science (SEECS) at National University of Sciences & Technology (NUST), Paksitan, from 2015-2016. He received his Ph.D. in telecommunications engineering from the Australian National University (ANU), Australia in 2013 and worked there as a Research Fellow from 2012-2015. His research interests are in the area of signal processing in wireless communication systems. He is an Associate Editor for IEEE WIRELESS COMMUNICATIONS LETTERS.

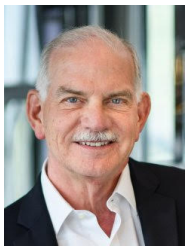

H. Vincent Poor (S'72, M'77, SM'82, F'87) received the Ph.D. degree in EECS from Princeton University in 1977. From 1977 until 1990, he was on the faculty of the University of Illinois at Urbana-Champaign. Since 1990 he has been on the faculty at Princeton, where he is currently the Michael Henry Strater University Professor. During 2006 to 2016, he served as the dean of Princeton's School of Engineering and Applied Science. He has also held visiting appointments at several other universities, including most recently at Berkeley and Cambridge. His research interests are in the areas of information theory, machine learning and network science, and their applications in wireless networks, energy systems and related fields. Among his publications in these areas is the forthcoming book *Machine Learning and Wireless Communications* (Cambridge University Press, 2021).

Dr. Poor is a member of the National Academy of Engineering and the National Academy of Sciences and is a foreign member of the Chinese Academy of Sciences, the Royal Society, and other national and international academies. Recent recognition of his work includes the 2017 IEEE Alexander Graham Bell Medal and the 2019 ASEE Benjamin Garver Lamme Award.

Eryk Dutkiewicz received his B.E. degree in Electrical and Electronic Engineering from the University of Adelaide in 1988, his M.Sc. degree in Applied Mathematics from the University of Adelaide in 1992 and his PhD in Telecommunications from the University of Wollongong in 1996. His industry experience includes management of the Wireless Research Laboratory at Motorola in early 2000's. Prof. Dutkiewicz is currently the Head of School of Electrical and Data Engineering at the University of Technology Sydney, Australia. He is a Senior Member of IEEE. He also holds a professorial appointment at Hokkaido University in Japan. His current research interests cover 5G/6G and IoT networks.